END

FILMED

DTIC

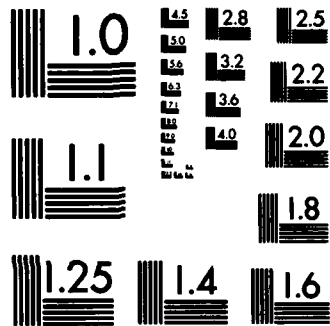| | 1.0 | | 4.5 | 2.8 | | 2.5 |
			5.0			
			5.6	3.2		2.2
			6.3			
				3.6		
	1.1		4.0			2.0
						1.8
1.25		1.4			1.6	

MICROCOPY RESOLUTION TEST CHART

NATIONAL BUREAU OF STANDARDS-1963-A

ⓖ

AD A122530

SIO REFERENCE SERIES

SIO Ref. # 81-16

NOTES ON THE DESIGN AND OPERATION CHARACTERISTICS

OF THE APPARATUS FOR THE EAST PACIFIC RISE

ELECTROMAGNETIC ACTIVE SOURCE EXPERIMENT

By: Peter D. Young

DEC 16 1982

A

Scripps Institution of Oceanography

University of California

November 1982

REPORT DOCUMENTATION PAGE		READ INSTRUCTIONS BEFORE COMPLETING FORM
1. REPORT NUMBER SIO Ref. #81-16	2. GOVT ACCESSION NO. AD22530	3. RECIPIENT'S CATALOG NUMBER
4. TITLE (and Subtitle) NOTES ON THE DESIGN AND OPERATION CHARACTERISTICS OF THE APPARATUS FOR THE EAST PACIFIC RISE ELECTROMAGNETIC ACTIVE SOURCE EXPERIMENT		5. TYPE OF REPORT & PERIOD COVERED
		6. PERFORMING ORG. REPORT NUMBER
7. AUTHOR(s) Peter D. Young		8. CONTRACT OR GRANT NUMBER(s) N00014-75-C-0999
9. PERFORMING ORGANIZATION NAME AND ADDRESS Scripps Institution of Oceanography La Jolla, CA 92093		10. PROGRAM ELEMENT, PROJECT, TASK AREA & WORK UNIT NUMBERS
11. CONTROLLING OFFICE NAME AND ADDRESS Office of Naval Research Arlington, VA 22217		12. REPORT DATE November 1982
		13. NUMBER OF PAGES 67
14. MONITORING AGENCY NAME & ADDRESS(if different from Controlling Office)		15. SECURITY CLASS. (of this report) Unclassified
		15a. DECLASSIFICATION DOWNGRADING SCHEDULE

16. DISTRIBUTION STATEMENT (of this Report)

Approved for public release. Distribution unlimited.

17. DISTRIBUTION STATEMENT (of the abstract entered in Block 20, if different from Report)

18. SUPPLEMENTARY NOTES

19. KEY WORDS (Continue on reverse side if necessary and identify by block number)

20. ABSTRACT (Continue on reverse side if necessary and identify by block number)

In April of 1979 an active source electrical conductivity sounding experiment was carried out near the East Pacific Rise at 21°N from aboard the R/V Melville as part of the RISE program (Spiess et al., 1980). The experiment and its conclusions are discussed in another paper (Young and Cox, 1981), but due to space limitations only the highlights could be presented. Accordingly, two monographs were written discussing this experiment in detail; one (Young, 1981) covers the mathematical . . .

DD FORM 1473 EDITION OF 1 NOV 65 IS OBSOLETE
1 JAN 73
S/N 0102-LF-014-6601

University of California at San Diego
Scripps Institution of Oceanography
La Jolla, California 92093

NOTES ON THE DESIGN AND OPERATION CHARACTERISTICS

OF THE APPARATUS FOR THE EAST PACIFIC RISE

ELECTROMAGNETIC ACTIVE SOURCE EXPERIMENT
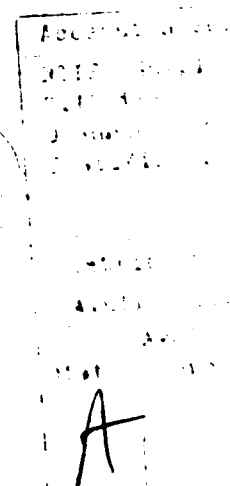
Peter D. Young

Scripps Institution of Oceanography
University of California at San Diego
La Jolla, California 92093

November 1982   SIO Reference number 81-16

Table of Contents

Introduction

In April of 1979 an active source electrical conductivity sounding experiment was carried out near the East Pacific Rise at 21°N from aboard the R/V Melville as part of the RISE program (Spiess et al., 1980). The experiment and its conclusions are discussed in another paper (Young and Cox, 1981), but due to space limitations only the highlights could be presented. Accordingly, two monographs were written discussing this experiment in detail; one (Young, 1981) covers the mathematical procedures used to interpret the data collected during the experiment, and the other, this document, describes the experimental apparatus, which was designed by Charles S. Cox and Tom Deaton and operated under their direction. It is hoped that this document will prove both interesting and useful.

Chapter 1

The Transmitter System Design

1. Introduction

The transmitter assembly may be considered to consist of four parts; the power supply and waveform control on shipboard, the cable delivering the power and the control signals from shipboard through roughly 3 kilometers of seawater to the transformer pressure casing near the seafloor, the electronics within this casing that transform and rectify the power coming down the cable and chop it into the waveform indicated by the control signals, and the lengths of cable lying along the ocean bottom that make up the transmitter antenna. The complete transmitter assembly is illustrated by figure 1.1 and its parts are described in the text of this chapter in reverse order, from the ocean bottom upward to the ship.
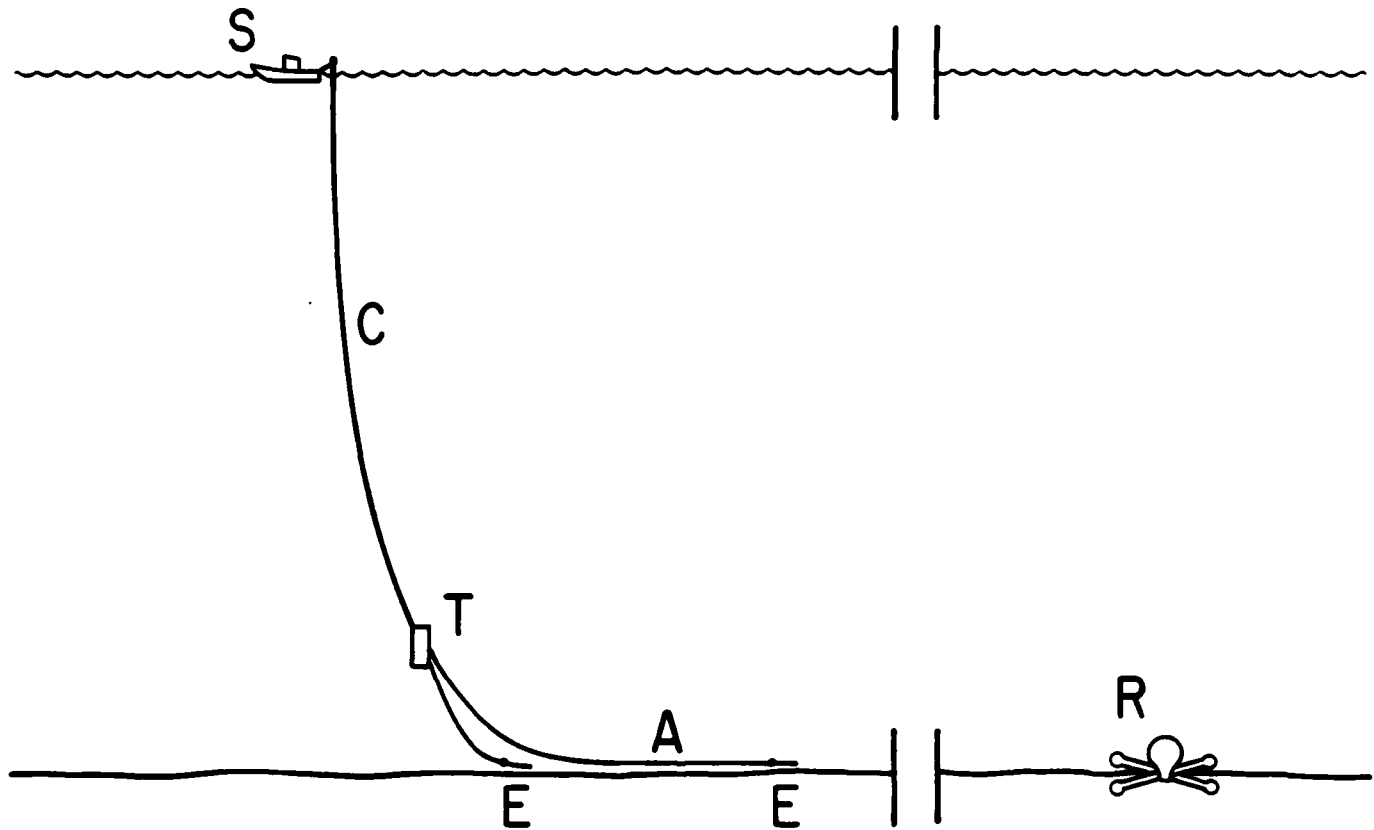
FIGURE 1.1

Experimental layout. C is the cable bringing 60 Hz power and high frequency control signals from the ship S, T is the transformer pressure casing, A is the insulated cable transmitter antenna, and E are the aluminum rod electrodes in contact with the seawater. R is the receiver instrument package, deployed 18.9 kilometers from the transmitter antenna.

2. The antenna cables

Two antenna cables come out of the pressure casing, both being insulated for their entire lengths except where they connect to short aluminum rod electrodes at their far ends. One of the cables is roughly 30 meters long, and the other is about 830 meters long, giving a length difference of 800 meters; when they lie parallel and a current flow is induced at the pressure casing from one cable to the other, they behave as a horizontal electric dipole 800 meters long. Each of the cables consists of a copper core 0.254 cm in radius, surrounded by a layer of plastic insulation 0.356 cm thick, which is in turn surrounded by a woven steel jacket (for structural reinforcement) with a mean thickness of 0.25 mm, with an outer plastic insulation layer 0.127 cm thick. The dielectric constant of the plastic insulating material is roughly 2. The electrode at the far end of each of the cables consists of three equal lengths of aluminum rod of diameter 0.6 cm, sequentially coupled together by means of a pair of clamps to give a total length for the electrode of 10 meters. The section of rod connecting directly to the cable end is so connected by means of a jointed clamp, and the junction is covered with insulating tape so that the seawater is completely excluded from the cable. The other end of the cable connects to the pressure casing through a bulkhead connector insulated from the seawater.

The aluminum rod electrodes, being exposed to the seawater during use, were subject to both chemical attack and electrode polarization, each of which could conceivably distort the transmitted signal. In practice, it turns out that the aluminum is not so much corroded as eaten away, so that, while the rod becomes smaller with time, it is always clean metal. In the experiment at the EPR the electrodes were immersed in operation for a period of about 5 hours, during which the rods would have decreased in diameter by less than 0.04 cm; for the purposes of the experiment the effect of this erosion should be negligible. The voltage drop across the seawater-aluminum interface due to polarization effects is frequency dependent, being greater at lower frequencies, but it was found that at worst this drop was no more than 3 volts per electrode; since the peak voltage applied to drive the current through the cables was in the neighborhood of 70 volts, the distortion of the transmitted signal voltage due to polarization effects is negligible.

3. The transformer pressure casing

The transformer pressure casing is a steel cylinder 51 cm tall and 31 cm in its outside diameter, and has walls 1.8 cm thick; in operation, it is filled with transformer oil, which serves both as electrical insulation and as reinforcement for the casing against outside pressure. The casing receives from its single input cable during normal operation 1500 volts peak-to-peak at 60 Hz, together with a control signal carrier at 180 KHz, initially 16 volts peak-to-peak at the shipboard end of the cable but attenuated to an estimated 0.5 volt peak-to-peak by the time it reaches the pressure casing; this latter signal may be modulated by 8 KHz and 16 KHz signals, which direct the shaping of the waveform of the current sent to the output cables. The control signal carrier is separated from the power frequency by means of a high-pass filter, and the power frequency is then fed to a large transformer that steps the voltage down to about 100 volts peak-to-peak with a peak-to-peak current in the neighborhood of 100 amperes. The transformed waveform is then rectified without smoothing, giving a waveform consisting of closely packed arches of the same sign. The 8 KHz and 16 KHz signals each control a silicon controlled rectifier, and the SCR's are set up to direct the rectified transformer output through the antenna cables in opposite directions when switched on by the presence in the casing input of their respective control signals; for example, if the two control frequencies were simultaneously present in the casing input, both SCR's would be turned on at the same time and an electrical short within the casing would result. This control system allows for only three states of current flow through the antenna cables (zero flow and positive and negative signs of a fixed amplitude), and the range of possible output frequency spectrums is limited to those associated with sequences of these three states in various durations within the period of the output waveform. The only way to alter the amplitude of the current delivered to the antenna cables (other than to shut it off) is to change the voltage of the power frequency delivered to the casing from shipboard, which is done by means of a hand-operated variable autotransformer aboard the ship.

One feature of the operation of a silicon controlled rectifier that is of considerable practical interest in this context is that, upon being turned on by its control input, it will not reset itself to its original nonconducting state until both the control input has been turned off and the current passing through it has fallen below a rather low threshold value, called its holding current (in this case, 0.1 amperes), if only briefly. What this means here is that the arches of the rectified transformer output cannot be smoothed out before this waveform is processed by the SCR's and fed into the antenna cables, and that after the control signal for an SCR has been removed from the casing's input cable one must still wait, as much as 120*th* of a second, until the base of an arch has been reached before the SCR shuts down. These effects are not in

themselves troublesome, as the high frequency components of the transmitter output resulting from the unsmoothed arches in the current waveform are attenuated by the seawater and rock to undetectability long before they can reach the receiver, and the effects on the output waveform of the SCR shutoff delay uncertainty fall in this same frequency range.

A more serious, and at the time of the experiment unanticipated, consequence of SCR latching resulted from the inductive properties of the antenna cables when fully deployed in seawater. The unexpectedly large inductance in the circuit (estimated in chapter 2 to be on the rough order of a millihenry) prevented the current flow through the SCR's from dropping low enough for unlatching after termination of their control signal, and as a result there was a continued short within the casing as soon as both SCR's had received their triggers, accompanied by arcing through the transformer oil. This problem was dealt with by altering the rectifier so as to remove every other arch in the rectifier output; the 120*th* of a second thus allowed for falloff of the inductively maintained current was sufficient to allow the SCR's to unlatch after removal of their control signals. The major disadvantage of this modification was that it emphasized the unwanted high frequency components at the expense of the low frequency components, thereby reducing the effective transmitter efficiency; if the efficiency of transmission is defined as the percentage of the total transmitted power going into the fundamental frequency and its third multiple, then the transmitter antenna current waveform that was originally planned would have given an efficiency of 91%, whereas this modification of that waveform should give an efficiency of 46%.

Perhaps as a consequence of damage sustained from the above problem, the SCR responsible for the negative portion of the output current waveform failed to turn on in response to its control signal about half of the time. As a consequence of the stacking procedure used at the receiver, irregularities between successive repetitions of the received signal tend to be averaged out, and so the effect on the recorded electrical field data of the instability in the transmitted waveform was the same as if a periodic waveform with half of the intended amplitude in its negative part had been transmitted. The symmetry properties of the waveform as originally planned were such that even multiples of the fundamental frequency would have had negligible amplitudes; the symmetry breakage resulting from the unplanned waveform modification did not alter the relations between the amplitudes and phases of the fundamental frequency and its odd multiples, but it did give rise to even multiples with significant amplitudes. These even multiples proved to have amplitudes too small to be of practical use, so this inadvertent waveform modification had the effect of a decrease in the transmitter efficiency. Assuming this waveform and supposing for the moment that the waveform modification discussed in the last paragraph has not been made gives an estimated transmitter efficiency of

82%, whereas if both waveform modifications are in effect, as is in fact the case, the transmitter efficiency is 41%.

4. The connecting cable

The cable connecting the pressure casing to the ship was an RG8/U coaxial cable, armored for structural support, and was provided by the Deep Tow project experimenters aboard the ship. This cable, deployable by winch, was 10 kilometers long; although only 3 kilometers of this cable was used by the active source experiment, signals could be inserted only at the cable's end at the shaft of the winch, and thus the power and control frequencies intended for the pressure casing had to travel the full length of the cable to reach it. The cable used a polyethylene insulation, making it resistant to compression by the extreme pressure at 3 kilometers depth, and had a nominal resistance per unit length of 3.9 ohms per kilometer and a nominal capacitance of 96.8 picofarads per meter.

5. The shipboard end

The part of the transmitter aboard ship had two parts; that responsible for the 60 Hz power frequency, and that responsible for the higher frequency waveform control signals. The power frequency was taken from the ship's main generator at 440 volts, run through a variable transformer assembly to give a voltage anywhere from 0 to 2000 volts, and sent down the cable to the pressure casing. The central part of the waveform control electronics is a collection of counting registers and logic that has the shape of the desired waveform hard-wired into it; the period of the waveform is determined by the oscillator that clocks this assembly, which can run at three different speeds to give the waveform periods of 4 seconds, 2 seconds, and 1 1/3 seconds respectively. The waveform generator has two outputs, which ultimately control the two SCR's in the pressure casing. Each of these outputs controls a square wave generator, one operating at 8 KHz and the other at 16 KHz, and the outputs of the two square wave generators are combined to form the input of a voltage controlled oscillator whose output is inserted into the cable leading to the pressure casing. The peak amplitude of the square waves coming from either of the square wave generators is fixed at a value that will produce 180 KHz from the the VCO; thus, since the waveform generator will only turn on one of the two square wave generators at a time, only a 180 KHz carrier frequency will be produced by the VCO.

Chapter 2

Order-of-Magnitude Estimates of Some of the

Transmitter Antenna Characteristics

1. Antenna cable parameters

Each of the antenna cables proceeding from the transformer pressure casing was comprised of four layers; a copper core, a layer of insulating plastic, a steel sheathing for strengthening purposes, and an outer plastic insulation layer. The copper core had a radius of 0.254 cm, the inner insulation layer had a thickness of 0.356 cm, the steel sheathing an average thickness of 0.025 cm, and the outer insulation layer a thickness of 0.127 cm. The permittivity ϵ_i of the insulating material can be taken as about $2\epsilon_0$, where ϵ_0 is the free space value, and its permeability μ_i can be taken as equal to the free space value μ_0. According to CRC (1974, p.D150), the steel of the sheathing can be taken to have a conductivity σ_s of 1.7×10^6 S/m, that of ductile cast iron, and the conductivity σ_c of the copper in the core is about 5.9×10^7 S/m. The copper will have a permeability essentially equal to the free space value; as for the sheathing, since steel is a ferromagnetic material, its magnetic permeability is technically undefined, but for the purposes of the following work we can reasonably assume a sheathing permeability μ_s of 500 μ_0 (taking into account that the sheathing material is braided steel rather than a uniform layer). The seawater surrounding the antenna has a conductivity σ_w of 3.2 S/m. The antenna consisted of two unmatched lengths of this cable, one being 800 meters longer than the other and both being tipped with aluminum rod electrodes 10 meters long apiece and about 0.6 cm in diameter.

2. Inductive and capacitive properties of the antenna-seawater system

For simplicity of calculation, the antenna will be considered to be a single arbitrarily long cable, surrounded on all sides by seawater; inductance and power emission will be calculated per unit length, and these values will then be multiplied by the 800 meter length of the antenna. The first assumption is not unreasonable, as even at the lowest frequency of 0.25 Hz the skin depth in seawater is about 550 meters, about two thirds the length of the antenna. The second assumption is more serious, as it just about doubles the number of paths of electrical conduction between the ends of the antenna; consequently, one should bear in mind that the inductance values calculated will be too high by a factor of roughly two, and must be scaled down accordingly. Electrical current will be assumed to be uniform over the length of the cable, as on the length scale and at the frequencies of interest the nonuniformity will be negligible; the electromotive forces applied to the cable will vary too slowly to effect any noticeable pileup of electrons anywhere over the length of the cable. The tacit assumption that the antenna is an 800 meter segment of an arbitrarily long cable implies that electrical current flows freely along the length of the steel sheathing; this is at odds with the fact that the sheathing is insulated from the seawater and the cable core at both ends of the cable. However, the sheath resistance per unit length of the cable is 0.060 ohm per meter, giving a total resistance of 52 ohms for 860 meters of cable; since the resistance of the seawater between the two electrodes, estimated in section 3, is roughly 0.2 ohms, it is apparent that it will make little difference to the calculations whether or not the sheath ends are insulated, as even in the uninsulated case the current flow through the sheath will be negligible compared to the flow through the seawater.

Drawing on the first section of Young, 1981, we start with Maxwell's equations,

$$\nabla \times \vec{E} = -i\omega\vec{B} \tag{2.1}$$

$$\nabla \times \vec{H} = \vec{J} + i\omega\vec{D} \tag{2.2}$$

$$\nabla \cdot \vec{D} = \rho \tag{2.3}$$

$$\nabla \cdot \vec{B} = 0 \quad , \tag{2.4}$$

where a time dependence of $e^{i\omega t}$ is assumed for the fields and currents, and the linearity conditions

$$\vec{D} = \epsilon\vec{E} \tag{2.5}$$

$$\vec{B} = \mu\vec{H} \quad , \tag{2.6}$$

where ϵ and μ are the electrical permittivity and magnetic permeability of the medium in question. If we express $\vec{J}$ in the form

$$\vec{J} = \vec{J_A} + \sigma \vec{E} \quad , \tag{2.7}$$

where the first term on the right is the part of the current density distribution that is driven by some source of EMF outside of the problem and the second term is the part that is ohmically induced within the material, whose electrical conductivity distribution is given by σ, by the electrical fields present within the problem, then (2.2) becomes

$$\nabla \times \vec{H} = \vec{J_A} + \frac{\gamma^2}{i\omega\mu}\vec{E} \quad , \tag{2.8}$$

where

$$\gamma^2 = i\omega\mu(i\omega\epsilon + \sigma) \quad . \tag{2.9}$$

We define a vector potential $\vec{A}$ such that

$$\vec{H} = \nabla \times \vec{A} \tag{2.10}$$

$$\vec{E} = i\omega\mu \left[\nabla \frac{1}{\gamma^2} \nabla \cdot \vec{A} - \vec{A} \right] \quad ; \tag{2.11}$$

if μ is taken to be a constant, then equation (2.1) is satisfied trivially. Substitution of (2.10) and (2.11) into (2.8) then gives

$$\nabla^2 \vec{A} - \gamma^2 \vec{A} - (\nabla \cdot \vec{A})\frac{1}{\gamma^2}\nabla(\gamma^2) = -\vec{J_A} \quad . \tag{2.12}$$

Adapting this equation to a cylindrical coordinate system gives

$$\nabla^2 \vec{A} - \gamma^2 \vec{A} - \hat{\rho}(\nabla \cdot \vec{A})\frac{1}{\gamma^2}\frac{d\gamma^2}{d\rho} = -\vec{J_A} \quad , \quad \gamma^2 = \gamma^2(\rho) \quad , \tag{2.13}$$

where $\vec{J_A}$ is a current distribution driven by some outside source of EMF, such as a shipboard generator; outside of the copper core of the cable we can set $\vec{J_A} = 0$.

In order to preserve translational symmetry of the fields with respect to the axis, and because there is no symmetrically preferred direction other than the axial direction, we must suppose a solution of the form

$$\vec{A} = \hat{z} \, F(\rho,\theta) \quad , \tag{2.14}$$

which reduces (2.13) to

$$\nabla^2 F(\rho,\theta) - \gamma^2 F(\rho,\theta) = 0 \quad . \tag{2.15}$$

Converting the ∇^2 operator to cylindrical form and making the separation

$$F(\rho,\theta) = R(\rho) \ T(\theta) \tag{2.16}$$

yields

$$\frac{d^2 T(\theta)}{d\theta^2} + \nu^2 \ T(\theta) = 0 \tag{2.17}$$

$$\frac{d^2 R(\rho)}{d\rho^2} + \frac{1}{\rho} \frac{dR(\rho)}{d\rho} - \left[\gamma^2(\rho) + \frac{\nu^2}{\rho^2} \right] R(\rho) = 0 \quad . \tag{2.18}$$

The added constraint that the fields must be rotationally symmetric about the axis eliminates all but the $\nu=0$ solution, giving

$$\vec{A} = \hat{z} \ R(\rho) \tag{2.19}$$

$$\frac{d^2 R}{d\rho^2} + \frac{1}{\rho} \frac{dR}{d\rho} - \gamma^2(\rho) R = 0 \quad . \tag{2.20}$$

If $\gamma^2(\rho)$ is constant over some range of ρ, then over that range equation (2.20) is solved by modified Bessel functions of zero order; this gives for the regions outside of the copper core

$$R_2(\rho) = A \ I_0(\gamma_2 \rho) + B \ K_0(\gamma_2 \rho) \tag{2.21}$$

$$\gamma_2^2 = -\omega^2 \mu_0 \epsilon_i = -2\omega^2 \mu_0 \epsilon_0 = -2\frac{\omega^2}{c^2} \tag{2.22}$$

for the inner insulation layer,

$$R_3(\rho) = C \ I_0(\gamma_3 \rho) + D \ K_0(\gamma_3 \rho) \tag{2.23}$$

$$\gamma_3^2 = i\omega\mu_s\sigma_s = 500 \ i\omega\mu_0\sigma_s \tag{2.24}$$

for the steel sheath,

$$R_4(\rho) = E \ I_0(\gamma_4 \rho) + F \ K_0(\gamma_4 \rho) \tag{2.25}$$

$$\gamma_4^2 = \gamma_2^2 \tag{2.26}$$

for the outer insulation layer, and

$$R_5(\rho) = G \ I_0(\gamma_5 \rho) + H \ K_0(\gamma_5 \rho) \tag{2.27}$$

$$\gamma_5^2 = i\omega\mu_0\sigma_w \tag{2.28}$$

for the seawater surrounding the cable. The physical constraint that $R(\rho)$ must vanish as ρ becomes arbitrarily large requires that

$$G = 0 \quad \text{if} \quad Re(\gamma_5) > 0 \tag{2.29}$$

or

$$H = 0 \quad \text{if} \quad Re(\gamma_5) < 0 \quad ; \tag{2.30}$$

the choices as to which of the two possible roots of γ^2 are to be used for each layer are arbitrary, in that different choices will give different solutions for the Bessel function coefficients, but the calculated field values will be the same for both the choices.

Inside of the copper core equation (2.13) cannot be conveniently used, as we wish the fields to be expressed in terms of the total current flow through the core rather than the externally driven current (which in this case is difficult to define anyway). To get a more appropriate equation, we start with the equation

$$\nabla \times \vec{H} = \vec{J} + i\omega\epsilon\vec{E} \quad , \tag{2.31}$$

derived from (2.2) and (2.5), where $\vec{J}$ is the total current density distribution, and make the substitutions (2.10) and (2.11),

$$\nabla \times \vec{H} = \nabla \times (\nabla \times \vec{A}) = \nabla(\nabla \cdot \vec{A}) - \nabla^2 \vec{A} \tag{2.32}$$

$$= \vec{J} + i\omega\mu\vec{E}$$

$$= \vec{J} - \omega^2\mu\epsilon \left[\left[\nabla \frac{1}{\gamma^2} \right] \nabla \cdot \vec{A} - \vec{A} \right] \quad ,$$

to get an equation for $\vec{A}$ with $\vec{J}$ as the source term. The same symmetry requirements that lead to (2.14) also apply in this case, and again we have for $\vec{A}$

$$\vec{A} = \hat{z} \, F(\rho, \theta) \quad , \tag{2.33}$$

from which we have

$$\nabla \cdot \vec{A} = 0 \quad , \tag{2.34}$$

and hence from (2.32)

$$\nabla^2 \vec{A} - \omega^2 \mu\epsilon \vec{A} = -\vec{J} \quad . \tag{2.35}$$

Defining, on the basis of the same symmetry requirements,

$$\vec{J} = \hat{z} \, J_C(\rho,\theta) \quad , \tag{2.36}$$

we then have

$$\nabla^2 F(\rho,\theta) - \omega^2 \mu \epsilon F(\rho,\theta) = -J_C(\rho,\theta) \quad . \tag{2.37}$$

At the frequencies involved in this problem the current distribution within the core should be essentially uniform across the core's cross-section, so if the core has a radius a and the total current passing through the core is I_C, then we have for J_C within the core

$$J_C = \frac{I_C}{\pi a^2} \quad . \tag{2.38}$$

As before, the physics of the problem requires that any solutions must be rotationally symmetric about the cylindrical axis (a condition required in any case by the constraint that the solution within the core be consistent at the core surface with the solution on the other side of this interface), and we therefore have from (2.37)

$$\vec{A} = \hat{z} \, R(\rho) \tag{2.39}$$

$$\frac{d^2R}{d\rho^2} + \frac{1}{\rho} \frac{dR}{d\rho} + \omega^2 \mu \epsilon R = -\frac{I_C}{\pi a^2} \quad . \tag{2.40}$$

A particular solution to (2.40) is

$$R(\rho) = -\frac{I_C}{\pi a^2 k^2} \quad , \tag{2.41}$$

where

$$k = \omega \sqrt{\mu \epsilon} = \frac{\omega}{c} \quad , \tag{2.42}$$

where c is the speed of light in the core (a bit less than that in vacuum), and the homogeneous solutions are regular Bessel functions of zero order; the requirement that the solution not become singular at the axis indicates that the proper homogeneous solution is a Bessel function of the first kind. In view of the above, we therefore have for the solution to (2.35)

$$\vec{A} = \hat{z} \, I_C \left[\chi \, J_0(k\rho) - \frac{1}{\pi a^2 k^2} \right] \quad , \tag{2.43}$$

where χ is a constant coefficient whose value is determined by consistency of the core and inner insulation layer solutions at the core surface.

The matching conditions at the various interfaces between the layers derive from the requirements that the tangential components of $\vec{E}$ and $\vec{H}$ be continuous across an interface. If $\vec{A}$ has the form

$$\vec{A} = \hat{z} \, R(\rho) \tag{2.44}$$

everywhere, then from (2.10) we have

$$\vec{H} = -\hat{\theta} \, \frac{dR}{d\rho} \tag{2.45}$$

and from (2.11) with (2.34) we have

$$\vec{E} = -i\omega\mu R \, \hat{z} \quad ; \tag{2.46}$$

hence, we have the conditions at an interface at $\rho = \rho_0$ between two layers

$$\mu_1 \, R_1(\rho_0) = \mu_2 \, R_2(\rho_0) \tag{2.47}$$

$$\frac{dR_1}{d\rho}\bigg|_{\rho_0} = \frac{dR_2}{d\rho}\bigg|_{\rho_0} \quad . \tag{2.48}$$

Either of the conditions (2.29) or (2.30) for the seawater solution will give, with the help of (2.47) and (2.48), the ratio between the coefficients E and F for the outermost insulation layer solution; by further, successive use of the interface matching conditions one can determine the ratio between the coefficients A and B for the inner insulation layer solution, and a final use of these conditions gives χ in terms of this ratio. The matching conditions then give the values of A and B, from which we have $\vec{A}$ everywhere. Not surprisingly, χ is a function of the frequency and the cable construction, but not of the current I_C. Note that, due to the condition that μ must be locally constant for either (2.13) or (2.35) to be valid, μ must be a constant everywhere except at the layer boundaries, where step changes from one layer to another are permitted.

The voltage V induced in a closed electrical circuit by a changing magnetic field $\vec{B}$ is given by

$$V = -\frac{d\Phi}{dt} \quad , \tag{2.49}$$

where

$$V = \int_C \vec{E} \cdot \vec{dl} \quad , \tag{2.50}$$

16

this being a line integral along the closed loop of the circuit, and

$$\Phi = \int_S \vec{B} \cdot \hat{n} \, da \quad , \tag{2.51}$$

this being a surface integral over the surface enclosed by the loop. For a physically rigid, stationary circuit in the absence of external magnetic fields the only changes in the magnetic flux Φ result from changes in the electrical current I going through the circuit, so (2.49) may in such cases be written in the form

$$V = -L\frac{dI}{dt} \tag{2.52}$$

$$L = \frac{d\Phi}{dI} \quad , \tag{2.53}$$

where L is called the magnetic inductance of the circuit. For the present problem we wish to compute the inductance per unit length, and for this purpose the proper surface of integration for the integral (2.51) is a rectangular strip of unit width, running parallel to the axis of the cable and extending from the axis out to infinity. Assuming all media in the system to be linear, we have

$$\vec{B} = \mu \vec{H} \tag{2.54}$$

and hence, from (2.45) and (2.51),

$$\Phi_0 = -\int_0^\infty \mu(\rho)\frac{dR(\rho)}{d\rho} \, d\rho \quad , \tag{2.55}$$

where Φ_0 is the flux through this rectangular strip. This may be rewritten as

$$\Phi_0 = -\int_0^\infty \frac{d\{\mu(\rho)R(\rho)\}}{d\rho} \, d\rho + \int_0^\infty R(\rho)\frac{d\mu(\rho)}{d\rho} \, d\rho \quad ; \tag{2.56}$$

bearing in mind that $\mu(\rho)R(\rho)$ is continuous across a layer boundary, we define

$$S(\rho) = \mu(\rho)R(\rho) \quad , \tag{2.57}$$

and (2.56) becomes

$$\Phi_0 = -\int_0^\infty \frac{dS(\rho)}{d\rho} \, d\rho + \int_0^\infty S(\rho) \frac{d\log\mu(\rho)}{d\rho} \, d\rho \quad . \tag{2.58}$$

Since by hypothesis the only place where $\mu \neq \mu_0$ is within the steel sheath, (2.56) becomes

$$\Phi_0 = \mu_0 R(0) + (\mu_s - \mu_0)\{R(\rho_1) - R(\rho_2)\} \tag{2.59}$$

where ρ_1 marks the inner boundary of the sheath and ρ_2 marks its outer boundary. As in this case the flux per unit length Φ_0 is directly proportional to the core current I_C, we have for L_0 the inductance per unit length

$$L_0 = \frac{\Phi_0}{I_C} \quad . \tag{2.60}$$

To get a reasonable estimate of the inductance L of the whole antenna, we multiply L_0 by 800 meters and divide by two.

The steel sheathing serves to strengthen the cable, but it also lowers the transmission efficiency of the antenna by absorbing part of the signal energy; the size of this effect may be estimated by Poynting vector calculations. The power P radiated through a surface S is given by

$$P = \int_S \vec{S} \cdot \hat{n} \, da \tag{2.61}$$

$$\vec{S} = \tfrac{1}{2} \operatorname{Re}\{\vec{E} \times \vec{H}^*\} \quad , \tag{2.62}$$

where $\vec{E}$ and $\vec{H}$ are as used in equations (2.1) and (2.2); from (2.45) and (2.46) we have

$$\vec{E} \times \vec{H}^* = -i\omega\mu \, R(\rho) \, \frac{dR^*(\rho)}{d\rho} \, \hat{\rho} \quad , \tag{2.63}$$

and if the surface is a cylindrical segment of length l and radius ρ, centered on the cable axis, then we have for P

$$\frac{P}{l} = \operatorname{Re}\left\{ -i\omega\mu\pi \, \rho \, R(\rho) \, \frac{dR^*(\rho)}{d\rho} \right\} \quad . \tag{2.64}$$

The sheath power absorption is most readily calculated by computing the net power flows per unit length through the core-insulation boundary and the insulation-seawater boundary, and then taking the difference between the two values, as the power absorption within the insulation layers is effectively zero.

Using the above formalism together with the cable design data provided at the beginning of this chapter, it was found that for a frequency of 1.0 Hz one gets $L_0 = 2.5 \times 10^{-5}$ *henry per meter*, giving an estimated inductance for the antenna at this frequency of L = 10 millihenries. Further calculations at a number of frequencies ranging up to 240 Hz suggest that the antenna inductance is virtually constant at this value over most of the range from 1.0 Hz up to 240 Hz. One exception to this that was discovered was an abrupt jump

to 18 millihenries at 60 Hz, followed by as abrupt a return to the 10 millihenry value at 64 Hz, and there may be other such anomalies over the frequency range from 1.0 Hz to 240 Hz that were missed by the search. The inductive reactance X_L is given by the expression

$$X_L = \omega L \quad , \tag{2.65}$$

X_L values of 0.063 Ω, 6.8 Ω, 7.5 Ω, 11 Ω, and 15 Ω at 1.0 Hz, 60 Hz, 120 Hz, 180 Hz, and 240 Hz respectively. In comparison, the electrical resistance of the copper core is 8.4×10^{-4} ohms per meter, or 0.72 ohms for the roughly 860 meters of the total antenna cable length; if the resistance of the seawater between the electrodes is taken to be 0.16 Ω, as estimated in the next section, and if an effective electrical resistance of 0.05 Ω due to polarization effects at the electrodes is assumed, then the total electrical resistance of the antenna-seawater system comes to 0.93 Ω.

For a simple inductive circuit consisting of a resistance in series with an inductance, both of whose values are independent of frequency, the inductive time constant is given by the quotient L/R; if the voltage driving an electrical current through the circuit is abruptly cut, the current will damp exponentially from its value at the time of cutoff, taking very close to 5 time constants to fall below 1% of the cutoff value. the inductance of the transmitter antenna on the seafloor being a function of frequency, a sudden cut in its driving voltage will not give a strictly exponential falloff of the antenna current, but a slightly distorted one; the calculated time constant over most of the frequency range is 11 milliseconds, whereas over the 60 Hz anomaly it is 19 milliseconds, allowing us to infer an initial approximately exponential current drop with the former time constant, blending into an approximately exponential tail with the latter time constant. In order to work, the modification discussed in section 1.3 that was made to avoid the SCR latching problem requires a 50 ampere current to drop below 0.1 ampere in less than 120th of a second, about 8.3 milliseconds; even assuming that any anomalous tails in the inferred transmitter antenna current decay curve can safely be ignored, the estimated decay time is still too long to meet this condition, by a factor of about 10. We infer that either the inductance of the transmitter antenna has been greatly overestimated, or the resistive and inductive properties of the pressure casing electronics must be taken into account in estimating the current decay curve.

Estimating the order of magnitude of the inductive backvoltage from the antenna which was mentioned earlier in this section, we have that for the intended antenna current waveform the current typically changed in increments of 50 amperes, with a rise or fall time of 240th of a second (see chapter 1), giving a rate of change of 6000 amperes per second. Multiplication of this by the estimated antenna inductance L at 60 Hz gives an upper limit for the

backvoltage of 11 volts.

The power radiation parameters of interest were also calculated for the frequencies 0.25 Hz, 1.00 Hz, and 2.25 Hz, and are most easily expressed in terms of the impedance per unit length Z_l,

$$Z_l = \frac{P}{I_c^2 l} \quad , \tag{2.66}$$

having units of ohms per meter. The impedance figures for net power flow across the core surface turn out to be 0.12, 0.50, and 1.1 microohm per meter for these respective frequencies, the bulk of which is dissipated in the seawater. Power dissipation within the sheath may be estimated by taking the difference between the net power flow out of the core boundary and the net power flow into the seawater from the outer insulation layer, as the insulation layers do not significantly absorb power, and when this is done we find that the sheath accounts for less than a thousandth of the total power loss; in view of the fact that the skin depth of the sheath material at 1.0 Hz is about 39 cm whereas the sheath is only a quarter of a millimeter thick on the average, the size of this fraction is not surprising.

Due to simplifying assumptions made in the previous derivation to expedite the calculation of the inductive properties of the antenna-seawater system, this work cannot be straightforwardly adapted to the calculation of the radial charge separation distribution within and about the antenna cable, and hence it is unsuitable for estimation of the capacitive properties of the antenna-seawater system. However, for the same reason that the antenna current could be assumed uniform over the length of the cable for the purposes of the derivation, within the frequency range of interest simple electrostatic modeling of the cable should estimate its capacitance properties without major error. For the sake of completeness, at least a rough estimate of these properties should be made, and this is done in the following paragraphs.

In computing the capacitance per unit length of the antenna cable, we take the conductivities of the core, sheath, and seawater to be arbitrarily large, thereby reducing the problem to that of two cylindrical capacitors connected in series, each using the plastic insulating material as dielectric. By skillful use of Gauss' law, Laplace's equation, and symmetry arguments, we have that the capacitance per unit length C_0 of a capacitor made from two concentric cylinders of radii a and b, where $a \geqslant b$, is

$$C_0 = \frac{2\pi\epsilon}{\ln(b/a)} \quad , \tag{2.67}$$

and from arguments based on charge conservation we have that the capacitance C of two capacitors C_1 and C_2 connected in series is

$$\frac{1}{C} = \frac{1}{C_1} + \frac{1}{C_2} \quad . \tag{2.68}$$

Bearing in mind that for the cable insulating material we have $\epsilon \approx 2\epsilon_0$, we thus have for the capacitance per unit length of the cable a value of 1.05×10^{-10} coulombs per volt-meter, or 105 picofarads per meter, giving a capacitance for an 800 meter length of cable of 0.084 microfarads. The capacitive reactance X_C is given by the expression

$$X_C = \frac{1}{\omega C} \quad , \tag{2.69}$$

which gives for an 800 meter length of cable reactance values of 1.9 $M\Omega$, 32 $K\Omega$, 16 $K\Omega$, 10.5 $K\Omega$, and 8 $K\Omega$ for the frequencies 1.0 Hz, 60 Hz, 120 Hz, 180 Hz, and 240 Hz respectively.

Whether an antenna is basically inductive or capacitive in nature is determined by the phase angle θ by which the current lags the voltage, given by the expression

$$\tan\theta = \frac{X_L - X_C}{R} \tag{2.70}$$

(Reitz and Milford, 1967, p.252); in a completely inductive system the current leads the voltage by 90°, and in a completely capacitive system the current lags the voltage by 90°. Using the value for R and the values at various frequencies for X_L and X_C given in this section, we find that for all of these frequencies the current leads the voltage by almost a full 90°, indicating a virtually completely inductive antenna, as the existence of the SCR latching problem suggests. At these frequencies the capacitive reactance is so large that capacitive effects have a negligible influence on the flow of current within the antenna-seawater system.

3. Electrical resistance of the seawater

The electrodes, as mentioned previously, are a pair of identical metal rods, each roughly 10 meters long and 0.6 cm in diameter, separated by a distance of 0.8 kilometer. If direct current were fed into the seawater through the electrodes, the current distribution would fan out very rapidly from the electrodes, so that over most of the distance between the electrodes the current would be spread over a large conducting cross-section, and hence most of the resistive power loss would take place in the close vicinity of the electrodes. Use of an alternating current would tend to constrict the electrical current distribution within the seawater to smaller distances about the antenna cable, but at the frequencies used in this experiment this effect, though appreciable, is not overwhelming, and its greatest effect is in the volume of seawater roughly intermediate in distance between the electrodes; the resistive power loss within, say, a hundred meters of each electrode would be affected to a very small extent, whereas the losses elsewhere within the seawater would merely be increased from insignificant to negligible. Accordingly, the DC resistance of the seawater is a reasonable approximation to the low frequency AC resistance, and should be strongly affected by the shape of the electrodes.

To simplify the calculations, it will be assumed that the electrodes are surrounded on all sides by seawater, allowing the use of cylindrical symmetry; the resistance value for the electrodes lying on the seafloor should be double the value calculated under this assumption, as replacing the half-space of comparatively nonconducting rock beneath the electrodes with seawater doubles the conductive cross-section in the problem. The calculational method to be used turns the resistance problem into a capacitance problem by use of a theorem that exploits a mathematical symmetry between charge separation within a capacitive system and current flow within a resistive system, and then a solution of the capacitive problem is drawn from various references. The system of units used in this section is rationalized MKS. The theorem, a simple proof of which may be found in Reitz and Milford (1967, pp.136-139), has that if C is the capacitance for a pair of conductors embedded in a dielectric medium with a permittivity of ϵ and R is the resistance for the same conductors in the same geometry embedded in a conductive medium of conductivity σ, then

$$R = \frac{\epsilon}{\sigma C} \quad . \tag{2.71}$$

From Smythe (1939, pp.37-39) we have that the electrostatic potentials V_1 and V_2 of two conductors of arbitrary shape embedded in a dielectric medium of permittivity ϵ and separated by a distance l much greater than either of their respective linear dimensions are given to first order by

$$V_1 = \frac{Q_1}{C_1} + \frac{Q_2}{4\pi\epsilon l} \tag{2.72}$$

$$V_2 = \frac{Q_2}{C_2} + \frac{Q_1}{4\pi\epsilon l} \quad , \tag{2.73}$$

where C_1 and C_2 are the respective capacitances of the two conductors taken individually with a second electrode at infinity and Q_1 and Q_2 are their respective charges; as the capacitance of a system is defined to be the ratio of the charge separation achieved to the voltage difference that did it, and as in this case $Q_2 = Q_1$, the capacitance C of the system of the two conductors is therefore

$$\frac{1}{C} = \frac{1}{C_1} + \frac{1}{2\pi\epsilon l} + \frac{1}{C_2} \quad , \tag{2.74}$$

and if b is the linear magnitude of the larger of the two conductors then the second order correction is at most of order $(b^2/2\pi\epsilon l^3)$. From (2.71) we then have for the resistance between the two conductors immersed in seawater

$$R = \frac{\epsilon_0}{\sigma_w} \left[\frac{1}{C_1} + \frac{1}{2\pi\epsilon_0 l} + \frac{1}{C_2} \right] \quad . \tag{2.75}$$

Smythe (1939, p.111), derives an integral expression for the capacitance of a conducting ellipsoid of general shape,

$$C = 8\pi\epsilon \left\{ \int_0^\infty [(a^2 + \theta)(b^2 + \theta)(c^2 + \theta)]^{-1/2} \, d\theta \right\}^{-1} \quad , \tag{2.76}$$

where a, b, and c are the lengths of the semiaxes, and if two of the three axes of the ellipsoid are equal in length the value of the integral is given in Grobner and Hofreiter (1966, p.32). While the capacitance of a cylindrical rod of finite length is complicated to calculate, such a rod can be reasonably well approximated by a long, narrow prolate spheroid, for which the solution is

$$C = \frac{8\pi\epsilon_0\gamma}{\ln\left\{ \frac{a+\gamma}{a-\gamma} \right\}} \quad , \tag{2.77}$$

$$\gamma = \sqrt{a^2 - b^2} \quad , \tag{2.78}$$

provided that the dielectric medium is free space, the long axis has a length of 2a, and the short axes have a common length of 2b. In the special case where $a \gg b$ we have

$$C \approx \frac{8\pi\epsilon_0\, a}{\ln\left\{\dfrac{4a^2}{b^2}\right\}} \quad : \tag{2.79}$$

if α is the length of the spheroid and β is the diameter, then from (2.75) we have to first order

$$R = \frac{1}{2\pi\sigma_w}\left[\frac{ln(4\alpha^2/\beta^2)}{\alpha} + \frac{1}{l}\right] \quad . \tag{2.80}$$

From CRC (1965, p.496) we have that the surface area S of a prolate spheroid for which $\alpha \gg \beta$ is to good approximation

$$S = \frac{\pi^2\alpha\beta}{4} \quad : \tag{2.81}$$

accordingly, for a prolate spheroid with the same length (10 meters) and surface area as one of the electrode rods we have $\beta = 0.76$ cm. If $\sigma_w = 3.2$ S/m, we then have from (2.80) that R = 0.078 Ω, which gives a seawater resistance value, corrected for the presence of the seafloor, of 0.16 Ω. This value is small compared to the resistance of the 800 meters of cable between the electrodes, and is roughly two to three times the estimated effective electrical resistance due to electrode polarization effects at the electrodes.

4. Relative power dissipations in seawater and crust

The upper limit on the efficiency of the transmitter for the purposes of the experiment is determined by the ratio of the power dissipations in the seawater and the crustal rock due to the action of the electric field produced by the transmitter antenna deployed on the ocean floor. It is not immediately obvious even whether this ratio is greater or less than unity, as, on the one hand, the high concentration of free charge carriers within the seawater should be strongly conducive to power dissipation therein, while, on the other hand, the sharp electrical conductivity differential at the interface between rock and water will tend to some extent to act as a mirror, reflecting energy emitted by the antenna downward to be absorbed by the rock beneath the ocean floor. Although detailed calculations based on the antenna design parameters are too tortuous to be practical, some light may be shed on the matter with some work with approximations.

The power dissipation p per unit volume of a material due to movement of charge carriers within the material under the influence of an externally generated electric field $\vec{E}$ is

$$p = \vec{J} \cdot \vec{E} \ , \tag{2.82}$$

where $\vec{J}$ is the electrical current mediated by the charge carriers (Reitz and Milford, 1967, pp. 297-299). When the current is induced by the electric field through ohmic processes, we have

$$\vec{J} = \sigma \vec{E} \ , \tag{2.83}$$

where σ is the electrical conductivity of the material, and hence

$$p = \sigma \vec{E} \cdot \vec{E} \ . \tag{2.84}$$

The total power P dissipated within a volume of not necessarily homogeneous material under the influence of an externally generated electric field $\vec{E}$ is then

$$P = \int_V \sigma(\vec{x}) \ \vec{E}(\vec{x}) \cdot \vec{E}(\vec{x}) \ d\vec{x} \ . \tag{2.85}$$

If we attempt to calculate the total power dissipated by a harmonic point horizontal electric dipole resting on the ocean floor, we find that p becomes singular at the dipole in such a way that the value for P calculated by using equation (2.85) is infinite; as one approaches the dipole arbitrarily closely, the electric field strength becomes arbitrarily large while the charge carrier density remains constant, causing the power density per unit volume to approach infinity about the dipole in a manner that cannot be finitely integrated over volume. This infinity is a direct consequence of the use of the mathematical abstraction of an infinitely large charge differential confined to an infinitely small region of space, and if the dipole is instead of finite

size, with electrodes of finite surface area, then the integral (2.85) has a finite, well-defined value. The lessons here are that the power loss associated with an electric dipole of a given dipole strength that is embedded in a conducting medium is a function of the details of its design, and that as the dipole becomes smaller the power dissipation is concentrated progressively closer to the dipole.

Although for a point dipole of finite strength the power dissipations P_s and P_c in seawater and crustal rock respectively are both infinite, their ratio R, where

$$R = \frac{P_s}{P_c} \quad ,$$
(2.86)

is a finite quantity; to be rigorous, one can consider R to be the limiting value of the power dissipation ratio for a dipole of fixed strength as the dipole dimensions are made arbitrarily small. Wait (1961) has derived a number of expressions for the electric field of a harmonic horizontal electric dipole in the presence of a conducting half-space, appropriate for various ranges of distance from the dipole, and his results are summarized in Kraichman (1970). Adapting Wait's work to the problem at hand, we have that for distances from the dipole of much less than a skin depth in seawater the electric field due to a harmonic point horizontal electric dipole of strength s and angular frequency ω at the ocean floor is given in cylindrical coordinates by

$$E_\rho = \frac{s \cos\phi}{\pi \sigma_s \rho^3}$$
(2.87)

and

$$E_\phi = \frac{s \sin\phi}{2\pi \sigma_s \rho^3}$$
(2.88)

for both above and below the interface,

$$E_z = -\frac{s \, i\omega\mu_0 \cos\phi}{4\pi\rho}$$
(2.89)

below the interface, and

$$E_z = -\frac{s \, i\omega\mu_0 \cos\phi}{4\pi\rho} \frac{\sigma_c}{\sigma_s}$$
(2.90)

above the interface, where σ_s is the electrical conductivity of the seawater and σ_c is the electrical conductivity of the crustal rock; calculating power dissipation integrals of the form (2.85) for the regions above and below the interface with these field expressions, leaving the lower limit of integration on the distance from the dipole undetermined, forming the power

dissipation ratio, and then determining its value as the undetermined limit of integration is allowed to approach zero gives

$$R = \frac{\sigma_s}{\sigma_c} \quad . \tag{2.91}$$

As σ_s at the ocean bottom is typically about 3.2 S/m, whereas the experiment indicated a mean value for σ_c of roughly three orders of magnitude less, it is seen that for an arbitrarily small dipole transmitter the absorption ratio is much greater than unity. This particular result is not directly applicable to the experiment, as the length of the transmitter antenna exceeds one skin depth of seawater at all frequencies used.

To estimate the magnitude of the power dissipation ratio for a transmitting antenna of finite size requires a more elaborate treatment, involving the integration of the power dissipation density over large volumes of water and rock about the antenna. Bannister (1981) has derived a single set of expressions for a harmonic point horizontal electric dipole in the presence of a conducting half-space, giving the electric field to good approximation over the distance range of from arbitrarily close to the dipole out to the beginning of the far field (distances much greater than a skin depth for the less conductive medium), and comparison of these expressions with Wait's expressions for the far field range permits their modification to cover all distances from the dipole. Adaptation of the modified Bannister expressions to the problem of a horizontal electric dipole of strength s resting on the floor of a semi-infinite ocean over a semi-infinite homogeneous crust gives for the electric field within the ocean ($z > 0$)

$$E_\rho = \frac{s \cos\phi \, e^{-\gamma_c\rho} e^{-\gamma_s z}}{2\pi\sigma_s\rho^3} \left\{ 2 + 2\gamma_c\rho + \gamma_c^2\rho^2 \right. \tag{2.92}$$

$$\left. - \frac{2\rho^2}{d^2} \left[1 - \frac{\rho}{\rho_i} e^{-\gamma_c(\rho_i-\rho)} \right] \right\} F(\rho) \quad ,$$

$$E_\phi = \frac{s \sin\phi \, e^{-\gamma_c\rho} e^{-\gamma_s z}}{2\pi\sigma_s\rho^3} \left\{ 1 + \gamma_c\rho + \frac{2\rho^2}{d^2} \left[1 - \frac{\rho}{\rho_i} e^{-\gamma_c(\rho_i-\rho)} \right] \right\} \quad , \tag{2.93}$$

and

$$E_z = -\frac{s \cos\phi \, e^{-\gamma_c\rho} e^{-\gamma_s z}}{2\pi\sigma_s\rho^2} \frac{\gamma_c^2}{\gamma_s} \left\{ \gamma_c\rho + \frac{\rho}{\rho_i} e^{-\gamma_c(\rho_i-\rho)} \right\} F(\rho) \quad , \tag{2.94}$$

where

$$\rho_i^2 = \rho^2 + d^2 \quad , \tag{2.95}$$

$$d = \frac{2}{\gamma_s} \quad , \tag{2.96}$$

$$\gamma_s^2 = i\omega\mu_0\sigma_s \quad , \tag{2.97}$$

$$\gamma_c^2 = i\omega\mu_0\sigma_c \quad , \tag{2.98}$$

and

$$F(\rho) = 1 - i(\pi\alpha)^{1/2} e^{-\alpha} \, erfc(i\alpha^{1/2}) \quad , \tag{2.99}$$

$$\alpha = -\frac{\gamma_c\rho}{2} \frac{\gamma_c^2}{\gamma_s^2} \quad , \tag{2.100}$$

$$erfc(x) = \frac{2}{\pi^{1/2}} \int_x^\infty e^{-u^2} \, du \quad , \tag{2.101}$$

and for the electric field within the crust $(z < 0)$ we have

$$E_\rho = \frac{s\cos\phi\, e^{-\gamma_c R}}{2\pi\sigma_s R^3} \left\{ \left[\left(\frac{3\rho^2}{R^2} - 1 \right)(1 + \gamma_c R) + \gamma_c^2\rho^2 \right. \right. \tag{2.102}$$

$$\left. \left. - \frac{2R^2}{d^2} \left[1 - \frac{R}{R_i}e^{-\gamma_c(R_i-R)} \right] \right] \right\} F(\rho) \quad ,$$

$$E_\phi = \frac{s\sin\phi\, e^{-\gamma_c R}}{2\pi\sigma_s R^3} \left\{ (1 + \gamma_c R) + \frac{2R^2}{d^2} \left[1 - \frac{R}{R_i}e^{-\gamma_c(R_i-R)} \right] \right\} \quad , \tag{2.103}$$

and

$$E_z = -\frac{s\, i\omega\mu_0 \cos\phi\, e^{-\gamma_c R}}{4\pi\rho R} \left\{ \gamma_c R d + z + \frac{R}{R_i}(d - z)e^{-\gamma_c(R_i-R)} \right. \tag{2.104}$$

$$\left. - \frac{\rho^2 d^2 z}{2R^4}(3 + 3\gamma_c R + \gamma_c^2 R^2) \right\} F(\rho) \quad ,$$

where

$$R^2 = \rho^2 + z^2 \tag{2.105}$$

and

$$R_i^2 = \rho^2 + (d - z)^2 \quad . \tag{2.106}$$

The effect of a transmitting antenna of finite size is simulated by defining a cutoff radius ρ_0.

and using ρ_0 in the field expressions in place of ρ in computing the electric field for $\rho < \rho_0$. Some numerical integration is involved in calculating the power dissipations above and below the ocean floor using the electric field expressions as altered in this manner, as the modified Bannister expressions are too complicated to make a completely analytical treatment worthwhile; the integration over ϕ may be done analytically both above and below the ocean floor, as can the integration over z within the crust, but for the other parameters of integration a numerical approach is indicated. For this experiment, if ρ_0 is taken to be half of the length of the transmitter antenna, then the power dissipation ratio should be estimated to within half an order of magnitude of the value that would be derived from a detailed consideration of the antenna design. Carrying out the indicated calculations for values of ρ_0 of 0.3 km, 0.4 km, and 0.5 km, assuming that $\sigma_s = 3.2$ S/m and $\sigma_c = 0.004$ S/m, we get for the ratio of seawater power dissipation to crustal rock power dissipation the values 306, 152, and 84.5 respectively, or 0.38, 0.19, and 0.11 times the value of R as given by (2.91), which in this case is 800. It appears that there is some advantage to an extended transmitter antenna, but that even for an antenna with a length on the order of a kilometer the bulk of the transmitted energy is nevertheless lost in the seawater.

Chapter 3

Receiver Design and Operating Characteristics

1. Introduction

From an external view (see figure 3.1), a receiver package is seen to consist of four parts; a spherical casing 61 cm in outside diameter, which is attached by a plate-like object of similar diameter at its bottom and a number of detachable electrical connections to a heavily weighted base, from which extend horizontally a crossed pair of electrode booms, each measuring 9 meters from end to end. The electrode booms consist of four 3 meter electrode supports of plastic pipe 6.0 cm in diameter projecting in a cross formation from the base, each of which is tipped on its outer end by a cylindrical Ag-AgCl electrode 8.9 cm in diameter and 26.4 cm long. These features are to be described in order and their operations discussed in the text of this chapter.
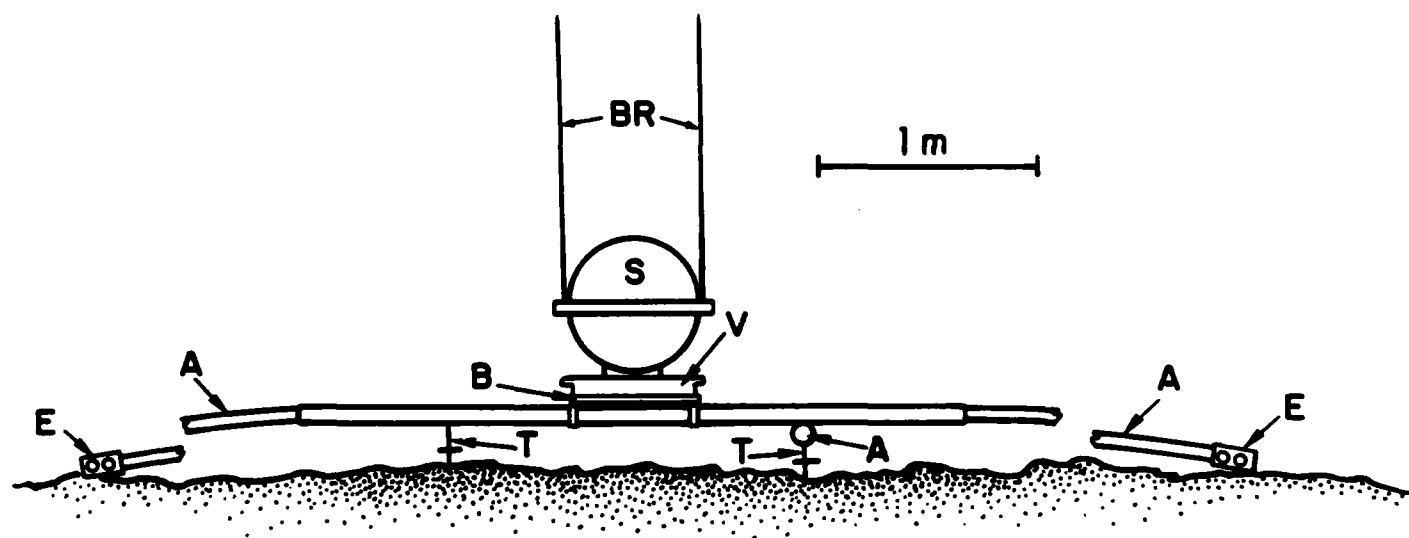
FIGURE 3.1

An external view from the side of the receiver instrument package.

2. The electronics housing

The housing consists of two painted aluminum hemispheres of wall thickness 2.5 cm joined at their mouths by an equatorial ring; the hemispheres were held together against the equatorial ring by a combination of straps and the pressure differential between the interior and the exterior. After assembly, the housing was pumped down to a pressure of about a third of an atmosphere. This served several purposes; it supplemented the straps holding the housing together while the package was waiting on deck to be submerged, it allowed easy checking for leaks, it would protect the contents of the housing from minor leaks by vaporizing the water as it entered, and it removed most of the moisture contained in the air within the housing, thereby preventing condensation when the sphere was cooled to the ambient temperature of the ocean floor. The housing was constructed and loaded in such a way that it had a substantial buoyancy (about 15 kilograms), so that upon its release from the weighted base after all measurements had been taken it would quickly float to the surface for recovery. Signals were passed to and from the electronics within the casing by means of electrical contacts passing through the equatorial ring, to which were attached on the outside a number of detachable electrical lines leading down to the weighted base.

3. The release mechanism

Between the housing and the weighted base was a pair of circular plates, held together by a vacuum seal; the housing was bolted to the top plate and the base was bolted to the bottom one. The volume between the plates contained a pair of small aluminum capillary tubes reaching through the top plate to the outside water and a pair of small explosive charges, one next to each of the tubes. The charges were to be fired by signals coming from a clock within the housing, two charges being used for the sake of redundancy; the idea was that at a time set within the package before its submersion the housing electronics would fire the charges, thereby destroying the seal between the plates and allowing the housing to drift to the surface, pulling itself loose from the detachable electrical connections to the base as it went.

4. The photographic compass

As well as the electrical field measurement electronics and the release timer electronics, the housing contained a device that photographically recorded the orientation and tilt of the receiver after its emplacement on the sea bed (its position relative to the transmitter and the ridge axis being determined to within 20 meters during its emplacement by reference to a pre-established transponder net). This device consisted of a standard hiker's compass suspended by a few wire supports from a gimbaled mounting over a piece of unexposed photographic film; a pinhole aperture, backed by a small electrically powered light source, is mounted at the center of the gimbaling, and the light source would be turned on for a brief interval whenever the cassette recorder was operated. The shadow images made on the film during the descent of the receiver package and the ascent of the housing were very faint compared to that made while the receiver package was in place on the seafloor, and the orientation and tilt of the receiver on the seafloor could be determined from the position on the film of this dark shadow. The lack of two or more such dark shadows would be adequate evidence that the receiver did not shift positions while on the bottom, and in the event that such a shift did occur a study of shadow intensities might be combined with irregularities in the cassette record to deduce the time of the shift and compensate for it in the analysis of the data. The compass assembly was contained within a sealed can that allowed the compass to measure a tilt of up to 10.2° in any direction.

5. The field measurement electronics

The leads from the electrodes at the ends of the booms were connected through the equatorial ring of the housing to a pair of low noise amplifiers, one amplifier for the electrodes of each boom. Amplifier noise is typically highest at low frequencies, tending to decrease and then level off with increasing frequency; this low frequency noise problem was circumvented in the receiver amplifier design by use of a special signal processing scheme. A signal input to the amplifiers, after passage through a 50 to 1 transformer, is first sent through a device that alternately inverts the sign of the signal and passes it unchanged, in a cycle with a frequency of 2 KHz; this processing shifts the information content of the signal well out of the high noise region of the amplifier's spectral response. The amplifier amplifies the processed signal by a factor of 2800, and the amplifier's output is sent through another alternating inversion device worked in synchronization with the first, thereby restoring the signal's original waveform. The signal is then passed through a low-pass filter to remove the high frequencies produced as an artifact of the chopping process (which are at this point well above the information-containing frequencies), and sent through a final amplification stage with a gain of 18. The overall gain of the whole amplifier system, allowing for the loss through filtering of unwanted harmonics, is close to 2.2 million, and the noise level in the system in the frequency range of from 0.25 Hz to 2.25 Hz is on the order of 1 nV^2/Hz. The schematic of the amplifier system is shown in figure 3.2.

The output of each amplifier went to a voltage-to-frequency converter that turned out a square wave train with a fundamental frequency linearly related to the input voltage. The VFC's were set to give a 4 KHz pulse train with an input of zero volts, and a frequency change of 4 KHz per volt. The output of each of the VFC's was sent to a bank of counting registers, with the VFC output fed for a short time interval into each of the registers in turn, with wraparound from the last register in the sequence to the first; provisions were made to temporarily store any pulse coming into the bank during the process of switching the VFC output from one register to the next in line. Each of the register banks contains 32 registers of 16 bits apiece, and the interval over which each received the output of the VFC was 1/8 of a second, giving a total scan time once through the bank of 4 seconds, or a cycling frequency of 0.25 Hz. The register bank cycling was in theory synchronized with the signal from the transmitter, as the transmitter waveform generator and the receiver register bank switching were driven by matched clocks that were synchronized shortly before the receiver was put overboard; unfortunately, the clock within the receiver was subject to a slow drift with respect to the clock aboard ship, enough so that synchronization between the two clocks was lost in the 5 days between the emplacement of the receiver on the ocean floor and the first activation of the
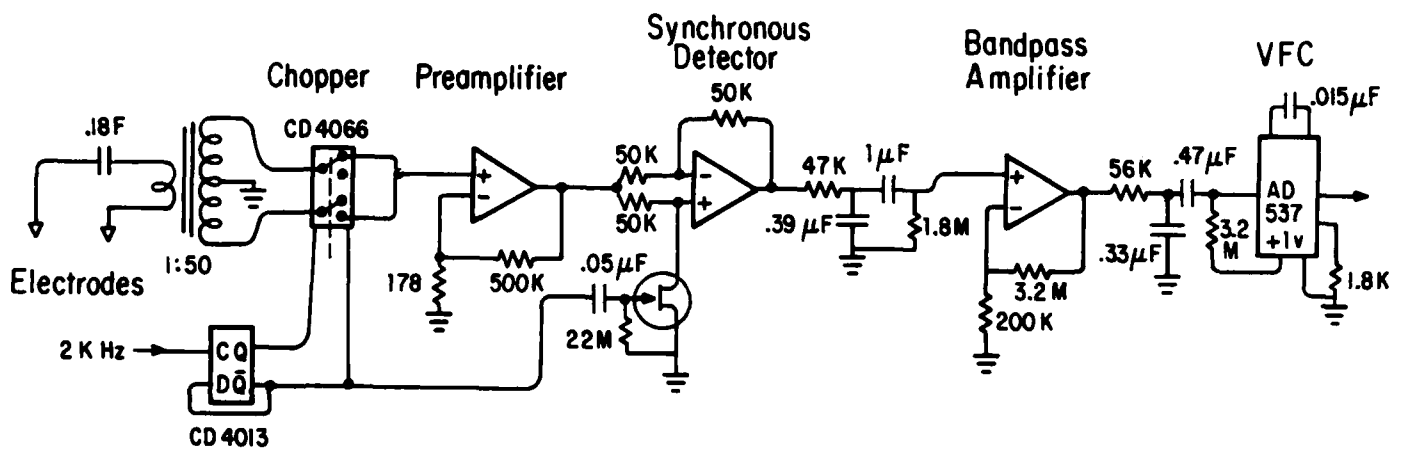
FIGURE 3.2

Schematic of the amplifier system for a single electrode pair.

transmitter antenna, but not enough to disrupt the signal stacking process within the receiver during the few hours in which the transmission was being monitored.

At fixed intervals the input to the banks (one bank for each electrode pair) would be halted, the contents would be read off onto a magnetic tape cassette, and the banks would be zeroed before the counting process would be restarted. For the receiver whose data was considered useful, the count-write cycle went as follows; 126 4 second counting cycles after the last register bank reset, 2 seconds of cassette recording, reset, one 4 second counting cycle, 2 seconds of cassette recording, and a final reset, for a total count-write cycle time of 512 seconds. The recording of the single 4 second counting cycle is for detection and correction of wraparound error in some of the registers during the preceding longer counting cycle, as it is possible with sufficiently high electric field intensities for a register in the bank to be incremented past its 16 bit capacity, causing it to reset to zero and start counting again up from there; in such a case, the sample over the shorter period will show which registers were at risk of overflow during the preceding sample, and will suggest the number of times an overflow reset occurred in each such register. Counting was halted during each operation of the cassette recorder because the operation of the recorder gives rise to enough electromagnetic noise within the housing to invalidate the count.

6. The recovery beacons

To aid in the housing's recovery after its release from the base, extending upward from the equatorial ring of the housing were two radio beacon antennas, set to broadcast on separate citizens band frequencies as soon as the housing surfaced. The electronics of the beacon transmitters is within the housing, and is activated by the loss of electrical conductivity between two contacts on each of the antennas as they are floated above the surface by the housing's buoyancy.

7. The power supply

The power supply for the housing electronics is a rack of 10 sealed lead-acid battery packs, each having linear dimensions of about 4 inches by 1 1/2 inches by 2 3/4 inches, with an operating voltage of 6 volts and a capacity of about 1 1/4 ampere-hours. The individual packs were hooked together in several groups, some in series and some in parallel, to provide the power at the appropriate voltages for the amplifiers, the register bank circuitry, the cassette recorder, the compass light, and the beacons. With all batteries fully charged, the receiver package can be expected to operate continuously for a period of at least 5 days but no more than 10 days, and the beacons should usefully transmit for about 2 weeks.

8. The base

The base is a loose rectangular structure of welded iron braces, roughly 60 cm by 90 cm by 5 cm and weighing about 18 kilograms, on the flat top of which was fastened a 27 kilogram anchor; the bottom vacuum plate was built into the anchor's top, and two 3 meter lengths of metal piping were bolted laterally onto this frame at right angles to each other to support the plastic electrode support piping. This plastic piping's outer diameter of 6 cm is a good match for the inner diameter of the metal support piping; a 3 meter length of plastic pipe was stuffed and cemented into each end of each of the support tubes, giving a total extension for each boom thus created of 9 meters between its electrodes. At each end of each of the booms was a Ag-AgCl electrode, the lead from each electrode being run through the plastic pipe and out of a hole in the metal support pipe, then going up to connect to the equatorial ring of the housing. The electrodes were each weighted with close to 3.6 kilograms of lead to hold them down against the bottom, preventing their movement by water currents.

9. The electrodes

The electrodes were of a type designed for use on the ocean bottom, being somewhat more resistant to shock than Ag-AgCl electrodes designed for laboratory use; a rough description of their construction is given in Filloux, 1973, and a discussion of noise considerations in their use is given in Filloux, 1974. In brief, each electrode consists of a silver gauge cylinder and stem packed in an electrode filler of diatomaceous earth and silver chloride within a porous container, which is in turn packed within a larger electrode housing using diatomaceous earth as the packing material; this is a change from the design given in the above references, which uses pyrex wool for this purpose. The manufacture of these electrodes has not yet been standardized, and the construction of a high quality electrode is still something of an art. Data on the internal noise of the electrodes in the frequency range covered by this experiment is not available, except in that the noise spectrum of the output of the amplifier system (see figure 3.7) appears to be dominated by the electronic noise from within the amplifier system.

10. Calibration

The spectral properties of the receiver electronics are either known or can be calculated, but not with the accuracy desired for the purposes of the experiment. Accordingly, the receiver electronics were calibrated with a known signal as input, so as to get transfer coefficients with which one could multiply the Fourier time series coefficients of the cassette records to get field values at various frequencies. The calibration signal had a 4 second period and an amplitude of roughly two tenths of a microvolt (an amplitude that increments several of the registers in the banks to near capacity while overflowing none of them), the waveform consisting of a null signal interrupted at some point in the period by a boxcar function with a duration of 1 second; the signal is fed into the appropriate antenna leads through resistors with resistances chosen to simulate the internal resistances of the electrodes.

If $f(t)$ is the electric field in volts per meter picked up across one of the receiver's electrode booms during operation on the seafloor, then we wish $f(t)$ to be expressed in the form

$$f(t) = \sum_{n=0}^{\infty} F_n \, exp(in\omega_0 t) \quad , \tag{3.1}$$

where ω_0 is the fundamental frequency of the waveform and the F_n are the spectral components of the measured component of the electric field. If the calibration signal $g(t)$ is expressed in the same manner, we have

$$g(t) = \sum_{n=0}^{\infty} G_n \, exp(in\omega_0 t) \quad , \tag{3.2}$$

where

$$G_n = A_n + i \, B_n \quad \text{for} \quad n \neq 0 \tag{3.3}$$

$$G_0 = \tfrac{1}{2} \, A_0$$

$$A_n = \frac{2}{T} \int_0^T g(t) \, cos(n\omega_0 t) \, dt \tag{3.4}$$

$$B_n = \frac{2}{T} \int_0^T g(t) \, sin(n\omega_0 t) \, dt \tag{3.5}$$

T being the period of the calibration waveform, equal to $\frac{2\pi}{\omega_0}$. There are simple analytical expressions for the G_n of the calibration waveform that was used. The data from the cassette recording is transformed according to the formula

$$X_m = \sum_{l=0}^{n-1} x_l \exp\left(-2\pi i \frac{lm}{n}\right) \quad , \tag{3.6}$$

where x_l is the recorded content of register l of the register bank, n is the number of registers in the bank, and X_m is the discrete finite Fourier transform of the register bank contents. If the x_l read from the record tape are derived from the calibration signal, then the desired transfer coefficients R_m are given by

$$R_m = \frac{G_m}{L X_m} \quad , \quad 1 \leqslant m < \frac{n}{2} \quad , \tag{3.7}$$

where L is the length of the boom separating the paired electrodes; it is present in (3.7) because $g(t)$ is a simulation of the voltage difference produced between an electrode pair due to their separation in an electric field. The coefficient R_0 is of dubious value, since the VCO feeding into each of the two register banks gives a nonzero frequency pulse train output for a null input, and the R_m for m greater than 15 are useless because of aliasing in the X_m.

Aliasing is a standard problem with discrete finite Fourier transforms, and is worth discussing in this context because it will prevent the determination of the spectral coefficients of any signal processed by the receiver electronics for frequencies of 4 Hz and above (which for the purposes of the experiment are of no interest), and can also cast doubt on some of the lower frequency determinations under certain circumstances. Let us suppose that we have a time series consisting of measurements taken at equal intervals, and let us take two separate transforms such as (3.6), calling them X_{m1} and X_{m2}, the latter using all of the measurements in the series, making n very large, and the former using only the first p measurements. Then the appearance of X_{m1} between m = 0 and $m = \frac{p}{2}$, if plotted against m, will be that of X_{m2} folded back and forth on itself between m = 0 and $m = \frac{p}{2}$, with each fold being accompanied by a complex conjugation of the spectral components past the fold, and the rest of the spectrum of X_{m1} will be alternate conjugated mirror images of this part of its spectrum. Examination of (3.6) gives us the relations

$$X_{m1} = X_{(m+p)1} \tag{3.8}$$

$$X_{m1} = X^*_{(p-m)1} \quad .$$

X_{m1} and X_{m2} will be identical in appearance if and only if both drop to zero and stay there before $m = \frac{p}{2}$ is reached. An attempt was made to give the receiver electronics a spectral response such that frequencies approaching or exceeding 4 Hz (the frequency corresponding to

$\frac{p}{2}$, since for the receiver electronics p=32 and the fundamental frequency is 0.25 Hz) would be severely attenuated before reaching the recorder, but unusually strong signals in this frequency range could interfere with proper translation of the data into field values. The calibration waveform does not have such a problem, so the transfer coefficients should be correctly estimated, but the same cannot be guaranteed for the measured electrical field signal; if this signal does in fact have inconveniently intense high frequency components, then some of the higher frequency field value estimates inferred from the recorded data could be rendered erroneous.

11. Electrode aging and calibration error

An unexpected problem in the calibration process was that the internal resistances of the electrodes were found to slowly increase with age. When the electrode resistances were first measured shortly after their construction, about a month before the experiment, the internal resistance of a typical electrode pair was fairly close to 5 Ω; however, when the internal resistances of the receiver package electrode pairs were measured again a few days before submersion of the package the resistances of the electrode pairs had gone up to about 10 Ω. As the electrodes could not be recovered after the experiment, the internal resistances of the electrode pairs could not be measured after use, and as it was reasonable to suppose that the 10 Ω measurement was an equilibrium value it was assumed at the time to be the actual electrode pair resistance during the receiver's operation on the sea bed. About a month later, measurements were made on some spare electrodes that had been kept in seawater, and a typical electrode pair resistance value was found to be 18 Ω. Linear interpolation with time between this measured value and the last gave a value of 15 Ω, which was used in the interpretation of the recorded data. The uncertainty as to the actual internal resistances of the receiver package's electrode pairs during their use is perhaps the most important unknown in the equipment parameters; the 15 Ω value is, on the available information, the best choice, but a value anywhere between 10 Ω and 18 Ω would not be unreasonable. To give the problem some perspective, the recorded data has been processed assuming electrode pair resistances of 5 Ω, 10 Ω, and 15 Ω, the field values estimated for these respective resistances being given in the following three tables, and some of these values are plotted in Argand diagram format in figure 3.3. A model consisting of a homogeneous half-space of rock under a half-space of 3.20 S/m seawater has already been fitted to the data processed under the assumption of a 15 Ω electrode pair resistance, giving a rock conductivity of 0.004 S/m as the best fit; similar fits for electrode resistances of 5 Ω and 10 Ω give rock conductivities of 0.006 S/m and 0.010 S/m respectively.

About a year after the experiment, measurements were made on a number of spare electrodes that had been preserved from the experiment, and i* was found that one electrode pair had retained its initial resistance of 5 Ω, although the other electrode pairs had somewhat higher internal resistances, with the resistance values scattered over a wide range.

TABLE 3.1

Transmitter-normalized experimental data, with an electrode resistance of 5 Ω assumed in its processing. Amplitudes are expressed in units of 10^{-6} nV/meter^2–ampere.

frequency	axis	modulus	phase	error radius
0.25 Hz	X	4.13	30.1°	0.26
0.25 Hz	Y	1.22	-59.4°	0.24
0.75 Hz	X	4.47	17.8°	0.32
0.75 Hz	Y	4.55	-75.6°	0.31
0.50 Hz	X	5.95	-157.2°	0.19
0.50 Hz	Y	2.60	122.1°	0.35
1.50 Hz	X	2.76	-153.3°	0.21
1.50 Hz	Y	5.50	99.5°	0.23
0.75 Hz	X	5.11	-81.9°	0.25
0.75 Hz	Y	3.66	-159.1°	0.30
2.25 Hz	X	1.54	147.1°	0.15
2.25 Hz	Y	4.09	30.4°	0.27

TABLE 3.2

Transmitter-normalized experimental data, with an electrode resistance of 10 Ω assumed in its processing. Amplitudes are expressed in units of 10^{-6} nV/meter^2–ampere.

frequency	axis	modulus	phase	error radius
0.25 Hz	X	3.80	19.3°	0.24
0.25 Hz	Y	1.10	-68.9°	0.22
0.75 Hz	X	2.88	8.8°	0.21
0.75 Hz	Y	2.79	-85.2°	0.19
0.50 Hz	X	4.16	-169.9°	0.13
0.50 Hz	Y	1.77	108.5°	0.24
1.50 Hz	X	1.68	-155.5°	0.13
1.50 Hz	Y	3.17	98.8°	0.13
0.75 Hz	X	3.29	-90.8°	0.16
0.75 Hz	Y	2.24	-168.7°	0.18
2.25 Hz	X	0.94	149.3°	0.09
2.25 Hz	Y	2.41	35.9°	0.16

TABLE 3.3

Transmitter-normalized experimental data, with an electrode resistance of 15 Ω assumed in its processing. Amplitudes are expressed in units of 10^{-6} nV/meter^2–ampere.

frequency	axis	modulus	phase	error radius
0.25 Hz	X	9.28	14.5°	0.59
0.25 Hz	Y	2.82	-75.0°	0.57
0.75 Hz	X	5.72	1.5°	0.41
0.75 Hz	Y	5.47	-95.5°	0.37
0.50 Hz	X	8.87	-178.6°	0.29
0.50 Hz	Y	3.88	96.8°	0.52
1.50 Hz	X	3.14	-159.1°	0.24
1.50 Hz	Y	5.60	96.5°	0.23
0.75 Hz	X	6.54	-98.2°	0.32
0.75 Hz	Y	4.40	-179.0°	0.36
2.25 Hz	X	1.72	148.0°	0.17
2.25 Hz	Y	4.28	39.8°	0.28

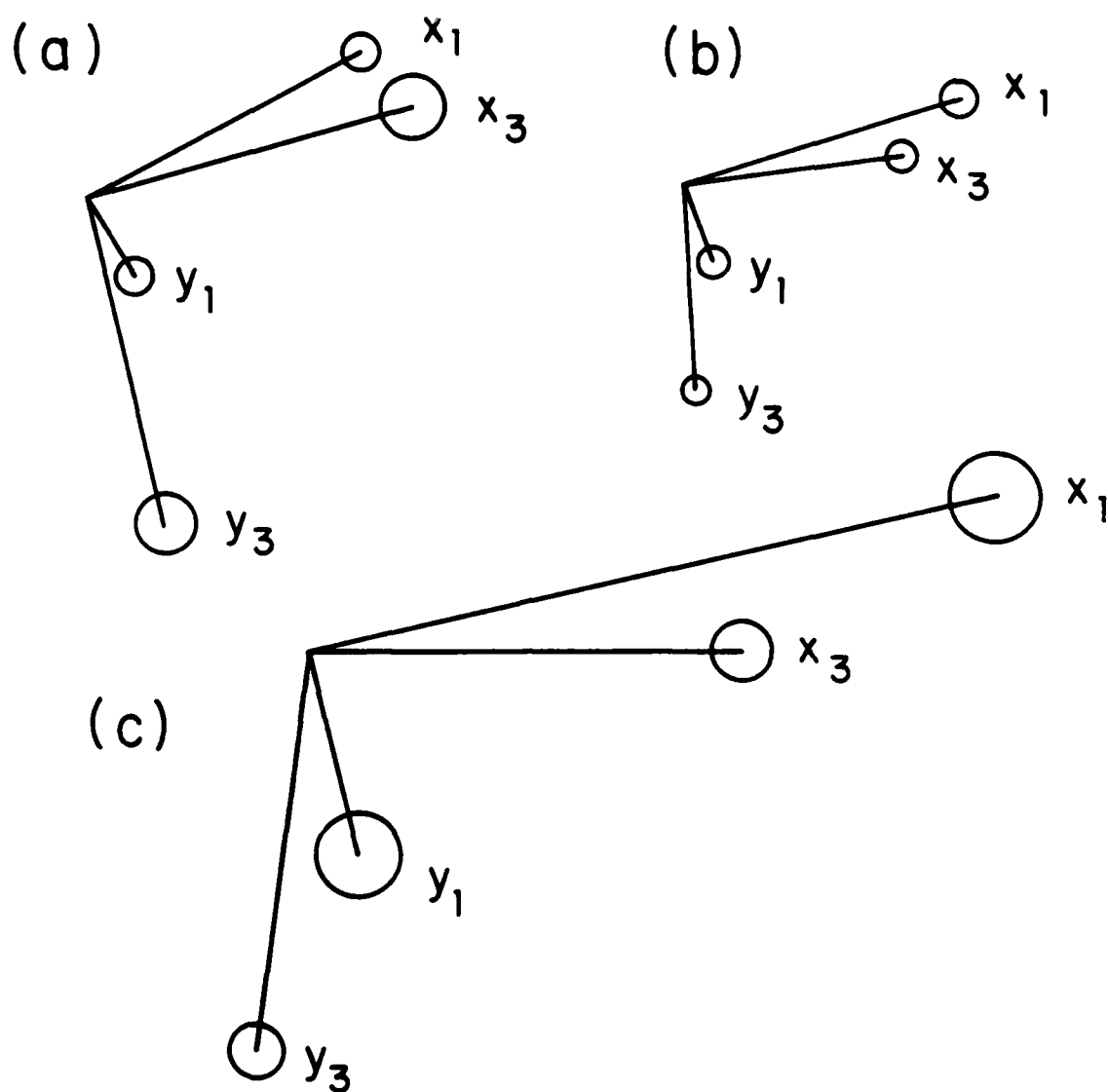FIGURE 3.3

Plots in Argand diagram format of the data in the lowest frequency data block processed assuming an electrode resistance of (a) 5 Ω, (b) 10 Ω, and (c) 15 Ω. The plots give relative magnitudes; see tables 3.1, 3.2, and 3.3 respectively for absolute magnitudes. The circle about each of the data points denotes an error of one standard deviation.

12. Spectral properties of the register bank circuitry

The transfer functions derived from the calibration procedure adjust for the spectral response characteristics of the electrodes, amplifiers, and register banks, but light can be shed on the process of inference of field values from the recorded data, particularly with reference to the aliasing problem, by a short analysis of the spectral properties of the register bank alone. Let us suppose that at time t_0 a counting cycle is started with all registers in the bank set to zero, and that during this cycle N complete sequential scans of the VCO output are made through the bank. Then the content $x(l,t_0)$ of register l in the bank after the cycle has been completed is given by

$$x(l,t_0) = \int_{-\infty}^{\infty} k(l,t) \, f(t+t_0) \, dt \tag{3.9}$$

$$k(l,t) = \sum_{j=0}^{N-1} h(t-jT-l\tau) \tag{3.10}$$

$$h(t) = H(t)H(\tau-t) \tag{3.11}$$

$$T = n\tau \tag{3.12}$$

where T is the time required for a single pass through the bank, n is the number of registers in the bank, H(t) is the step function, and f(t) is the VCO counting rate as a function of time. If $X(m,t_0)$ is the discrete finite Fourier transform of the register bank contents as in (3.6), then we have from (3.9)

$$X(m,t_0) = \int_{-\infty}^{\infty} p(m,t) \, f(t+t_0) \, dt \tag{3.13}$$

$$p(m,t) = \sum_{l=0}^{n-1} k(l,t) \, \exp\left(-2\pi i \frac{lm}{n}\right) \quad . \tag{3.14}$$

If we define the continuous infinite Fourier transforms

$$F(\omega) = \int_{-\infty}^{\infty} e^{-i\omega t} \, f(t) \, dt \tag{3.15}$$

$$f(t) = (2\pi)^{-1} \int_{-\infty}^{\infty} e^{i\omega t} \, F(\omega) \, d\omega \tag{3.16}$$

and

$$P(m,\omega) = \int_{-\infty}^{\infty} e^{-i\omega t} \, p(m,t) \, dt \tag{3.17}$$

$$p(m,t) = (2\pi)^{-1} \int_{-\infty}^{\infty} e^{i\omega t} \, P(m,\omega) \, d\omega \quad , \tag{3.18}$$

then substitution of (3.16) and (3.18) into (3.13) with use of the delta function definition

$$\delta(x-y) = (2\pi)^{-1} \int_{-\infty}^{\infty} e^{ik(x-y)} \, dk \tag{3.19}$$

gives

$$X(m,t_0) = (2\pi)^{-1} \int_{-\infty}^{\infty} e^{i\omega t_0} \, P(m,-\omega) \, F(\omega) \, d\omega \quad . \tag{3.20}$$

To calculate $P(m,\omega)$ we define

$$G(t_1,\omega) = \int_{-\infty}^{\infty} e^{-i\omega t} \, h(t-t_1) \, dt \quad , \tag{3.21}$$

which has the solution

$$G(t_1,\omega) = \frac{ie^{-i\omega t_1}(e^{-i\omega\tau}-1)}{\omega} \quad , \tag{3.22}$$

giving for $P(m,\omega)$

$$P(m,\omega) = \sum_{l=0}^{n-1} \sum_{j=0}^{N-1} G(jT+l\tau,\omega) \, \exp\left[-2\pi i\frac{lm}{n}\right] \tag{3.23}$$

$$= \frac{i(e^{-i\omega\tau}-1)}{\omega} \, q(N,-\omega T) \, s(n,m,-\omega\tau)$$

$$q(N,x) = \sum_{j=0}^{N-1} e^{-ixj} \tag{3.24}$$

$$s(n,m,x) = \sum_{l=0}^{n-1} \exp\left[-il\left(2\pi\frac{m}{n}+x\right)\right] \quad . \tag{3.25}$$

The function $q(N,-\omega T)$ is a periodic function of ω with a period of ω_0 as defined earlier. At integer multiples of ω_0 it has a tall peak with a real amplitude of N, and between any two such adjacent peaks there are N-1 zeros equally and symmetrically spaced with a spacing interval of $\frac{\omega_0}{N}$; for the rest of its period the function's largest modulus is considerably smaller than its maximum at the tall peak (the larger the value of N, the smaller the maximum modulus in the low amplitude region between two of the tall peaks). The function

$s(n,m,-\omega\tau)$ follows the same pattern, but n replaces N, the period is $n\omega_0$, the spacing interval for the n-1 zeros between two of the large peaks is ω_0, and the large peaks are offset from integer multiples of $n\omega_0$ by an amount $m\omega_0$. If $q(N,-\omega T)$ and $s(n,m,-\omega\tau)$ are multiplied together, for integer m the large peaks of s will always coincide with large peaks of q, but the large peaks of q that do not coincide with large peaks of s coincide with zeros of s. If N is much larger than n, as is the case for the receiver electronics (N=126 as compared to n=32), then the large peaks of q will be very sharp in comparison with those of s, and a peak of the product function will have a width at its base (defined as the distance between the two zeros flanking the peak) of $2\dfrac{\omega_0}{N}$ and a height of nN; if the product peak is approximated by an isosceles triangle with this base width and height, the area under the peak will be $n\omega_0$. As the modulus of the product function will be considerably smaller everywhere in the region between the peaks than at the peaks (with a mean amplitude in this region that is even smaller), if the function $F(\omega)$ is reasonably smooth over the widths of the product peaks we can make the approximation

$$q(N,-\omega T)s(n,m,-\omega\tau) = n\omega_0 \sum_{j=-\infty}^{\infty} \delta\{\omega-(jn+m)\omega_0\} \quad . \tag{3.26}$$

Putting (3.26), (3.23), and (3.20) together, we get

$$X(m,t_0) = i\ n\ (2\pi)^{-1} \left\{\exp\left[-2\pi i\frac{m}{n}\right]-1\right\} \tag{3.27}$$

$$\times \sum_{j=-\infty}^{\infty} \frac{\exp\{i(jn+m)\omega_0 t_0\}}{(jn+m)}\ F\{(jn+m)\omega_0\}$$

where $m\neq0$; if $m=0$, the same holds, except that the $j=0$ term is replaced with $F(0)$. Since $f(t)$ is a real function, we have from (3.15) that $F(-\omega)=F^*(\omega)$, and between this and (3.27) the aliasing effect mentioned earlier is illustrated.
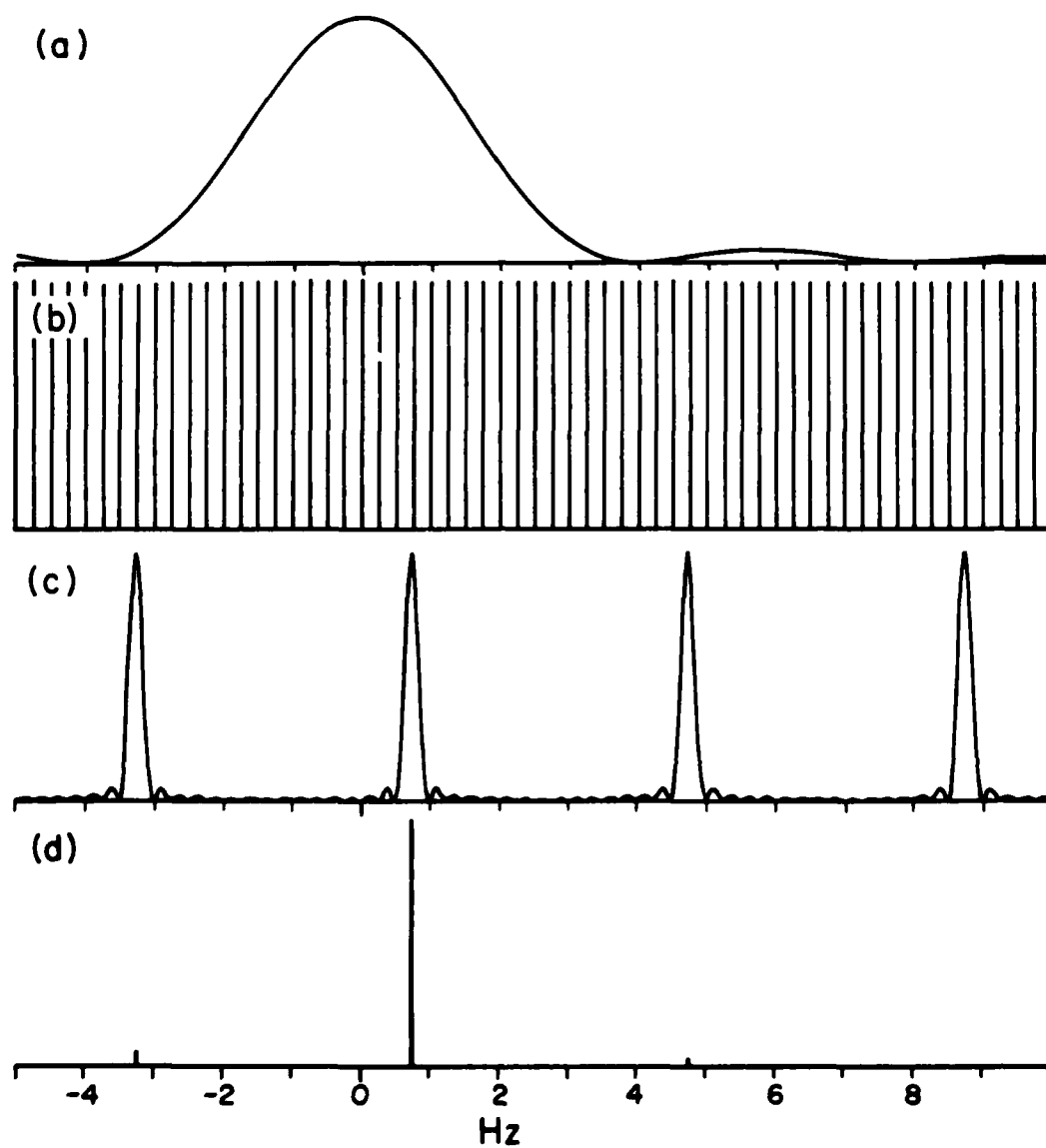
FIGURE 3.4

Components of $|P(m,\omega)|^2$ from -5.0 Hz to 10.0 Hz, with m=3, n=16, N=126, and τ=0.25 second. (a) is the envelope function, (b) is $|q(N,-\omega T)|^2$, (c) is $|s(n,m,-\omega\tau)|^2$, and (d) is their product $|P(m,\omega)|^2$. Vertical scales are not the same. $(2\pi)^{-1}|P(m,\omega)|^2$ is the kernal of integration that maps $S(\omega)$, the power spectrum of the register bank input, into $<X(m,t)X^*(m,t)>$.

13. Discretization error

The previous discussion assumes for mathematical convenience that the VCO counting rate is a continuous function (as in fact the voltage controlling it is), whereas it is actually a series of discrete pulses, each pulse being a standardized quantum of integrated voltage standing for the integration of the VCO input voltage over the time span between that pulse and the one immediately previous. Because of this quantization process, in the switching of the VCO output from one register in the bank to the next in line, an integration over the time span containing the register transition has its value credited entirely to either one register or the other, when this value should properly be split between the two registers; the result is called a discretization error. We wish to estimate the size of the error for each register in the bank after a full counting cycle of N passes through a bank of n registers, the correlation between the errors for the different registers in the bank, and how discretization error is reflected in the discrete Fourier transform of the bank contents.

The situation is analogous to one in which a machine spins a continuous length of string at a rate proportional to a control voltage, the string comes knotted at regular intervals of length, and at regular intervals of time a mark is put on the string where it comes out of the outlet orifice; the measured length of the string between any two successive marks is then directly proportional to the integral of the control voltage over the time interval denoted by the markings, and the number of knots between the marks is equivalent to the digitized equivalent to the integral. It is seen from this picture that if s is the length of string between two given sequential marks and d is the length of string between two sequential knots, then the error introduced by using the knot count between the marks as a measure of s can never exceed $\pm d$. One can, in principle, arbitrarily reduce the error by arbitrarily reducing the size of d, but there is no practical advantage to be gained by reducing d much past the point where its size is comparable to one standard deviation of the integral of the control voltage over the interval between two sequential marks. To simplify the mathematics, it will be assumed in the following discussion that d is in fact somewhat smaller than this noise parameter, and this assumption will subsequently be verified for the case of the receiver in operation on the seafloor.

Let x be the error introduced by the digitization approximation, and let us consider a length s of the string between two sequential marks. Let y be the remainder of the division s/d, so that $0 \leqslant y \leqslant d$, and let ϕ be the phase of the knot sequence on this length of string with respect to the first of the two marks to have come out of the machine. We then find that x is a function only of y and ϕ, with no dependence on s other than that implied by the value of y. We define $\phi = 0$ to correspond to the case in which the nearest knot to the reference mark is up against the right side of the mark (so that the knot is just within the interval of string in

question), and $\phi=2\pi$ to correspond to the case where the nearest knot to the reference mark is up against the left side of the mark (just outside the interval); in the former case the error will be (d-y), and in the latter case it will be -y.

In illustration, we consider the case in which s=3.75d, for which y=0.75d, for various values of ϕ. Referring to figure 3.5, we see that if ϕ happens to be in the range from 0 up to $3\pi/2$ there are 4 knots between the marks, giving a length estimate exceeding the actual value of s by 0.25d; however, if ϕ is anywhere between $3\pi/2$ and 2π the knot count between the marks is reduced to 3, giving an estimate for s that is short by the amount 0.75d. This argument is easily generalized for all y to the rule

$$x = \begin{cases} (d-y) & , \quad 0 \leqslant \phi < \theta \\ -y & , \quad \theta \leqslant \phi < 2\pi \end{cases} \tag{3.28}$$

$$\theta = 2\pi(y/d) \quad , \tag{3.29}$$

illustrated in figure 3.6. The average of x over ϕ for fixed y is zero.

The phase ϕ, being an artifact of an arbitrary choice at the start of the run as to where in the first length d of string after the first mark the first knot should be tied, will have a uniform probability distribution over the range $0 \leqslant \phi \leqslant 2\pi$ for a statistical ensemble of runs with identical noiseless voltage profiles, although the ϕ parameters for successive marked intervals of string will have the same relative values for every run. With this in mind, we have from (3.28) and (3.29) the probability distribution g(x,y) of x for fixed y

$$g(x,y) = p_1(y) \, \delta\{x-(d-y)\} + p_2(y) \, \delta(x+y) \quad , \tag{3.30}$$

$$0 \leqslant y < d$$

$$p_1(y) = y/d \quad , \quad p_2(y) = 1 - y/d \quad . \tag{3.31}$$

Now taking noise in the control voltage into account by use of the assumption that one standard deviation of s is much larger than d, we have that y also has a uniform probability distribution over its range for a statistical ensemble of runs, giving for the probability distribution f(x) of x

$$f(x) = \begin{cases} \dfrac{d-|x|}{d} & \text{if } -d \leqslant x \leqslant d \\ 0 & \textit{otherwise} \quad . \end{cases} \tag{3.32}$$

Having f(x) the probability distribution of the error for a single pass through a register in the bank, we can compute F(N,x) the probability distribution of the cumulative digitization
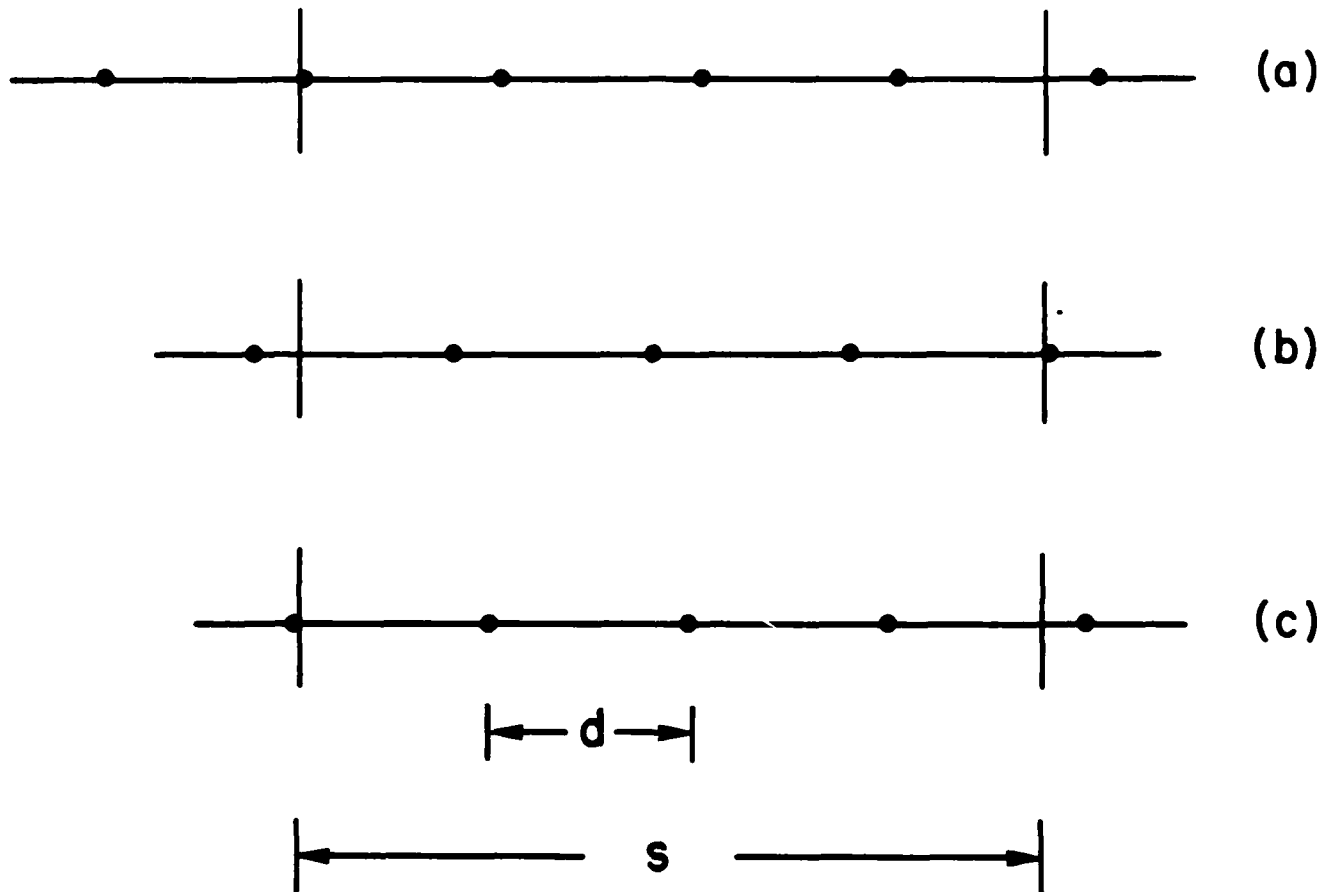
FIGURE 3.5

Illustration of the case $s = 3.75d$, for (a) $\phi = 0$, (b) $\phi = \frac{3\pi}{2}$, and (c) $\phi = 2\pi$, with errors of $x = 0.25d$, $x = -0.75d$, and $x = -0.75d$ respectively.
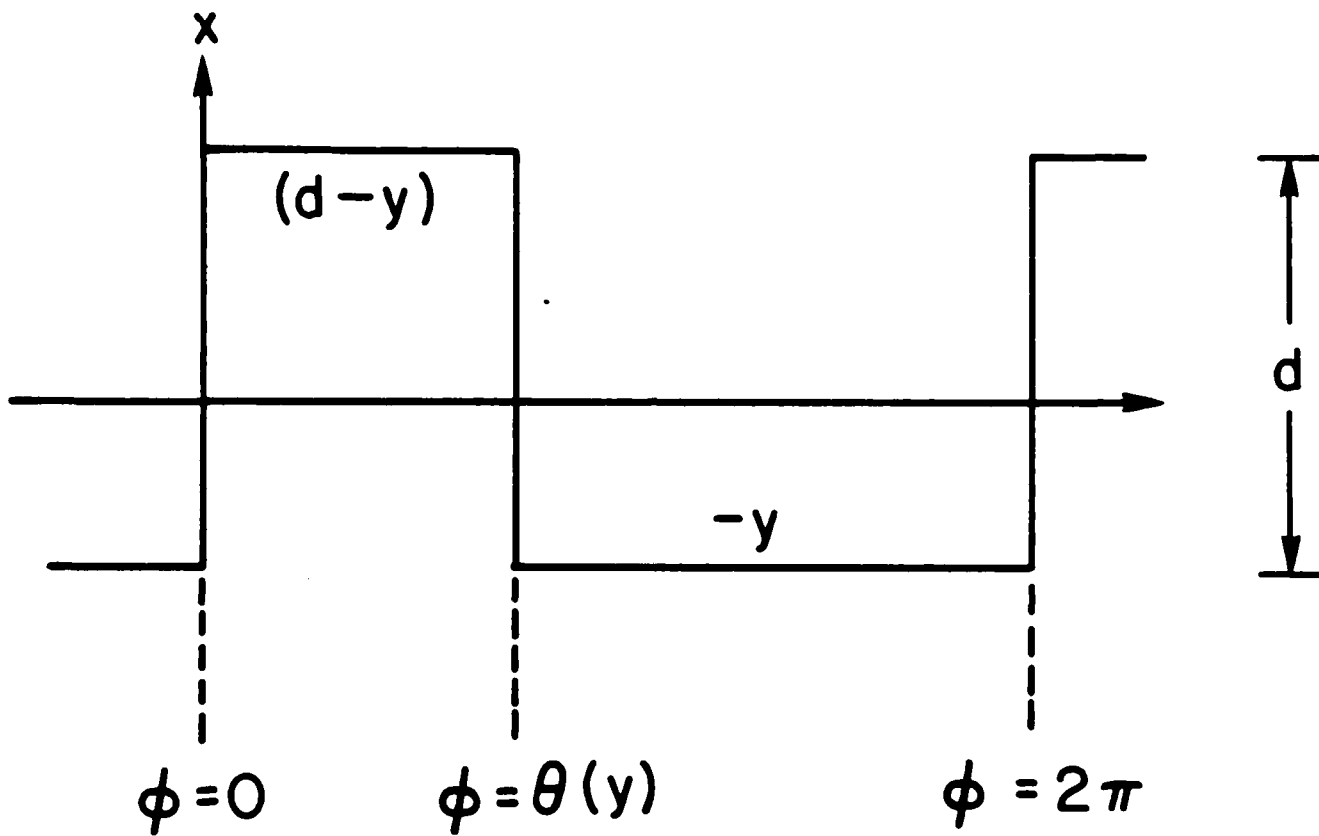
FIGURE 3.6

Illustration of the discretization error function of the remainder y and the knot phase ϕ, as given by equations (3.28) and (3.29).

error after N passes through the register by use of the formulas

$$F(N,x) = (2\pi)^{-1} \int\limits_{-\infty}^{\infty} e^{-ikx} \, A(N,k) \, dk \qquad (3.33)$$

$$A(N,k) = B^N(k) \qquad (3.34)$$

$$B(k) = \int\limits_{-\infty}^{\infty} e^{ikx} \, f(x) \, dx \quad , \qquad (3.35)$$

taken from Chandrasekhar (1943). These formulas deal with the one-dimensional random walk problem, where N is the total number of steps and $f(x)$ is the probability distribution for a single step; a critical assumption in their use is that the individual steps be uncorrelated with each other, a condition that is met in the problem at hand provided that the assumption made previously about the magnitude of the control voltage noise holds. These formulas can be generalized to deal with probability distributions in any number of dimensions by replacing the Fourier transform expressions in (3.33) and (3.35) with their equivalents for the desired dimensionality.

The central limit theorem states that for sufficiently large N the distribution $F(N,x)$ should closely approach a Gaussian distribution irrespective of the shape of $f(x)$. Since in the present problem $f(x)$ already bears a noticeable qualitative resemblance to a Gaussian distribution, sufficiently large N to give $F(N,x)$ a shape indistinguishable to the eye from a Gaussian distribution will certainly be a lot less than 126. Knowing in advance that $F(N,x)$ should be for practical purposes a Gaussian distribution and that the Fourier transform of a Gaussian is another Gaussian, we can save a considerable amount of work by fitting a Gaussian to $B(k)$ about $k=0$ and carrying this Gaussian through the subsequent steps leading to $F(N,x)$; that $B(k)$ will usually not look very much like a Gaussian should not affect the validity of the final answer. When this is done, we get

$$F(N,x) = \frac{1}{\sqrt{2\pi\sigma^2}} \exp\left[-\frac{x^2}{2\sigma^2}\right] \qquad (3.36)$$

$$\sigma^2 = \frac{2}{3} \, N \, d^2 \quad , \qquad (3.37)$$

giving

$$< x(l) \, x(l) > = \sigma^2 \qquad (3.38)$$

for the self-correlation of the error in register l.

Although the phases for the different marked string intervals in our model all have uniform probability distributions over their ranges, their values relative to each other are well-determined; if ϕ_i is the phase for the ith interval and y_i is the remainder for this interval, then for ϕ_{i+1} we have

$$\phi_{i+1} = \phi_i - 2\pi(y_i/d) \quad , \tag{3.39}$$

since a count excess in one register is at the expense of adjacent registers. If x_1 and x_2 denote the errors for two adjacent registers after a single pass through the bank, then we can use this relation to get a probability distribution $g(x_1,x_2,y_1,y_2)$ of x_1 and x_2 for fixed y_1 and y_2 analogous to (3.30), with the form

$$g(x_1,x_2,y_1,y_2) = p_1(y_1,y_2) \, \delta\{x_1-(d-y_1),x_2-(d-y_2)\} \tag{3.40}$$

$$+ \, p_2(y_1,y_2) \, \delta\{x_1+y_1,x_2-(d-y_2)\}$$

$$+ \, p_3(y_1,y_2) \, \delta(x_1+y_1,x_2+y_2)$$

$$+ \, p_4(y_1,y_2) \, \delta\{x_1-(d-y_1),x_2+y_2\} \quad ,$$

with the sum of p_1, p_2, p_3, and p_4 equal to one for all y_1 and y_2 within their proper ranges. If the probability distributions for y_1 and y_2 are taken to be uniform within their ranges and uncorrelated, as one would expect in this problem, by integration of this function over these variables we can get $f(x_1,x_2)$ the probability distribution of the errors in two adjacent registers after a single pass through the bank. Then using the two-dimensional equivalents of formulas (3.33) through (3.35), we get $F(N,x_1,x_2)$ the probability distribution for the cumulative correlated errors after N passes through the bank, from which we calculate

$$< x(l) \, x(l\pm1) > = -\frac{Nd^2}{12} = -\frac{\sigma^2}{8} \quad , \tag{3.41}$$

the correlation between the errors of two adjacent registers after N passes through the bank. The calculations leading up to this result are long and tedious but straightforward. Similar work for nonadjacent registers indicates that the effect of noise on the contents of even a single intervening register is sufficient to destroy all correlation between the errors in the nonadjacent registers for any number of passes, giving

$$< x(l) \, x(m) > = 0 \quad , \quad l\neq m \text{ and } l\neq m\pm1 \quad . \tag{3.42}$$

Putting together (3.38), (3.41), and (3.42), we get for the correlation between the elements of the discrete Fourier transform of the errors in the register bank contents after N

passes through the bank

$$<X(j)X(k)> = \sum_{l=0}^{n-1} \sum_{m=0}^{n-1} <x(l)x(m)> \exp\left\{-2\pi i\left(\frac{jl-km}{n}\right)\right\}$$ (3.43)

$$= \begin{cases} \frac{2}{3} nNd^2 [1 - \frac{1}{4} \cos(2\pi k/n)] & \text{if } j=k \\ 0 & \text{otherwise} \end{cases}$$

The largest error is seen to occur at $k=n/2$, in the spectral range of least interest.

We have that if r is the change in the VCO's output frequency with a unit change in the input voltage, then the quantum of integration d represented by a VCO pulse is

$$d = \frac{1}{r} \quad .$$ (3.44)

If τ is the period per pass during which a register receives the VCO output, and $n(t)$ is the noise component of the VCO input, then the noise integral I for one pass will be

$$I = \int_{-\infty}^{\infty} h(t) \, n(t) \, dt \quad ,$$ (3.45)

where $h(t)$ is as defined by (3.11). Assuming that $n(t)$ is a stationary series of zero mean value (a valid assumption for any true noise), $<I>$ the mean of I over an ensemble of passes

$$<I> = \int_{-\infty}^{\infty} h(t') <n(t'-t)> dt' \quad ,$$ (3.46)

where t is an averaging parameter, will be zero, and $<I^2>$ will be

$$<I^2> = \int_{-\infty}^{\infty} dt' \int_{-\infty}^{\infty} dt'' \, h(t') \, h(t'') <n(t'+t)n(t''+t)>$$

$$= \int_{-\infty}^{\infty} dt' \int_{-\infty}^{\infty} dt'' \, h(t') \, h(t'') \, R(t'-t'')$$ (3.47)

$$R(t') = < n(t) \, n(t-t') > \quad ,$$ (3.48)

where $R(t')$ is the autocorrelation function of $n(t)$. By its nature $R(t')$ is of necessity an even function for any stationary series. If we make the definitions

$$S(\omega) = \int_{-\infty}^{\infty} e^{-i\omega t} R(t) \, dt \quad ,$$ (3.49)

$$R(t) = (2\pi)^{-1} \int_{-\infty}^{\infty} e^{i\omega t} S(\omega) \, d\omega \quad , \tag{3.50}$$

$$G(\omega) = \int_{-\infty}^{\infty} e^{-i\omega t} h(t) \, dt \quad , \tag{3.51}$$

$$h(t) = (2\pi)^{-1} \int_{-\infty}^{\infty} e^{i\omega t} G(\omega) \, d\omega \quad , \tag{3.52}$$

we have from (3.47) by substitution

$$<I^2> = (2\pi)^{-1} \int_{-\infty}^{\infty} G(\omega) \, G(-\omega) \, S(\omega) \, d\omega \quad , \tag{3.53}$$

and by reference to (3.21) and (3.22) we have

$$G(\omega) = \frac{i \, (e^{-i\omega\tau} - 1)}{\omega} \tag{3.54}$$

$$<I^2> = \pi^{-1} \int_{-\infty}^{\infty} \frac{1 - \frac{\cos(\omega\tau)}{\omega^2}}{} S(\omega) \, d\omega \quad . \tag{3.55}$$

That R(t) is real and even gives $S(\omega)$ the same properties, allowing us to write

$$<I^2> = \frac{2}{\pi} \int_{0}^{\infty} \frac{1 - \cos(\omega\tau)}{\omega^2} S(\omega) \, d\omega \quad . \tag{3.56}$$

The autocorrelation spectrum $S(\omega)$, which is also called the power spectrum, is for this problem given by figure 3.7 up to 3.75 Hz; this is the sum of the power spectra of the ocean bottom electrical noise and the electrical noise from the electrodes and the housing electronics, the latter having a value on the order of 1 nV^2/Hz over the frequency range (0.25 Hz to 3.75 Hz) covered by this figure. Linearly extrapolating the segment of this graph between 0.25 Hz and 0.50 Hz to zero frequency and making the unrealistically conservative assumption of a cutoff in $S(\omega)$ past 3.75 Hz, for $\tau = 0.25$ seconds (the value of τ appropriate to the receiver electronics) we get a value for $<I^2>$ from (3.56) of 0.4 (nV/Hz)^2, which is roughly 44 times larger than the value of 9×10^{-3} (nV/Hz)^2 estimated for σ^2, the discretization error for an ensemble average of single passes through the bank. This is given by

$$\sigma^2 = \frac{2}{3} d^2 \quad , \tag{3.57}$$

which is taken from equation (3.37), where d is given by expression (3.44). From section 3.5 we have that the VCO's were set for a frequency change of 4 KHz per volt; allowing for the
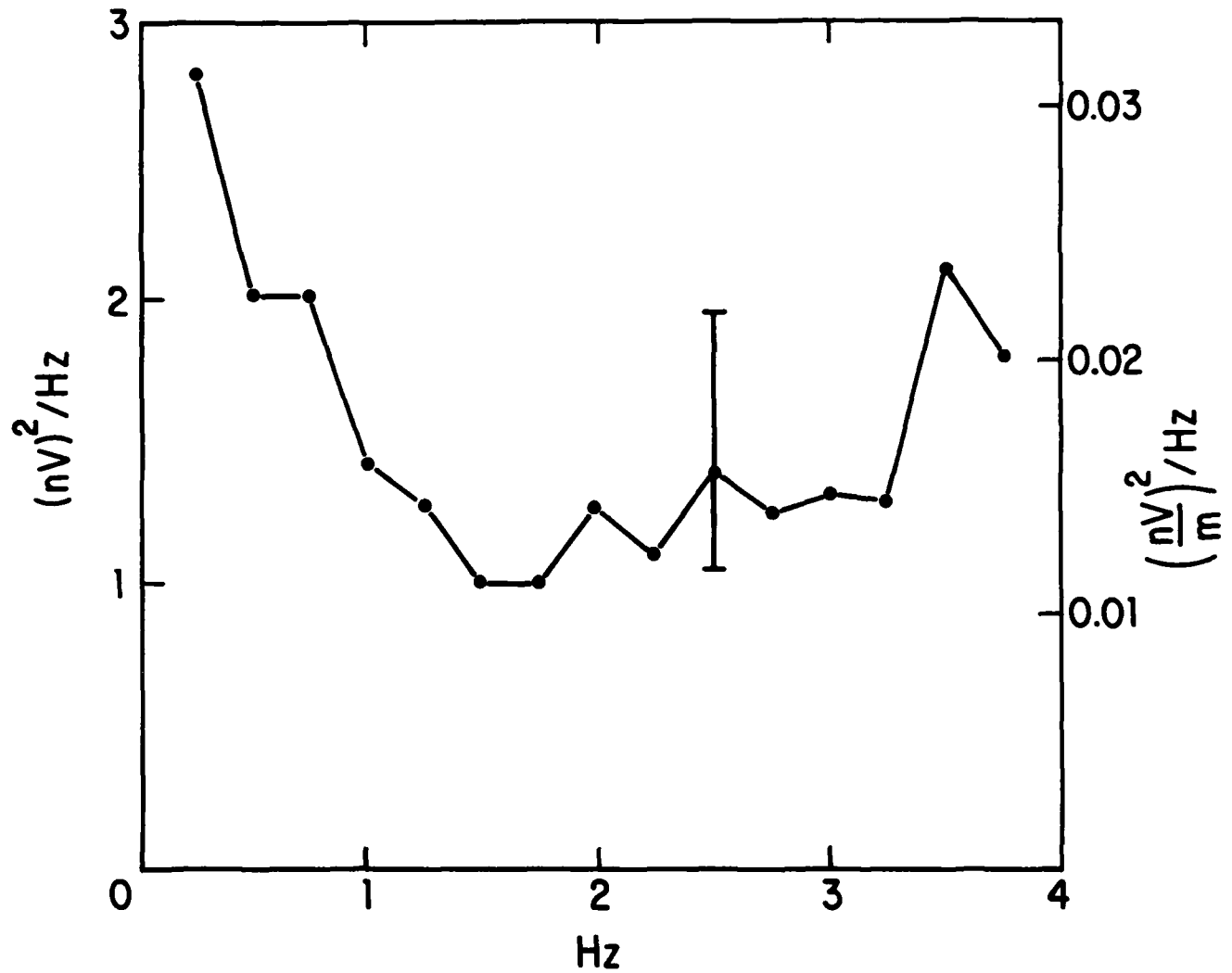
FIGURE 3.7

The power spectrum recorded by the receiver during a period when no signal was being transmitted. Compiled by Adam Schultz from experimental data.

amplification by the preceding electronics by a factor of 2.2×10^6, we get $r = 8.8$ Hz/nV, and hence (before rounding to one significant figure) $d = 0.114$ nV/Hz. This justifies the assumption made at the end of the second paragraph of this section, that the increment of discretization d is much smaller than the rms noise of the integrated input voltage.

References

Bannister, P. R., Image theory EM fields of horizontal dipole antennas in presence of conducting half-space, Naval Underwater Systems Center Technical Report 6511, 18 September 1981.

Chandrasekhar, S., Stochastic problems in physics and astronomy, Reviews of Modern Physics, 15, 1-89, 1943.

CRC (The Chemical Rubber Company), *Handbook of Chemistry and Physics*, 55th Edition, CRC Press, 1974.

CRC (The Chemical Rubber Company), *Standard Mathematical Tables*, 14th Edition, The Chemical Rubber Company, 1965.

Filloux, J. H., Techniques and instrumentation for study of natural electromagnetic induction at sea, Phys. Earth Planet. Inter., 7, 323-338, 1973.

Filloux, J. H., Electrical field recording on the sea floor with short span instruments, J. Geomag. Geoelectr., 26, 269-279, 1974.

Grobner, W. and N. Hofreiter, *Integraltafel*, Part 2, Springer-Verlag, Wein and New York, 1966.

Kraichman, M. B., *Handbook of Electromagnetic Propagation in Conducting Media*, U. S. Government Printing Office, 1970.

Reitz, J. R., and F. J. Milford, *Foundations of Electromagnetic Theory*, Addison-Wesley Publishing Company, 1967.

Smythe, W. R., *Static and Dynamic Electricity*, First Edition, McGraw-Hill Book Company, New York and London, 1939.

Spiess, F. N., K. C. Macdonald, T. Atwater, R. Ballard, A. Carranza, D. Cordoba, C. Cox, V. M. Diaz Garcia, J. Francheteau, J. Guerrero, J. Hawkins, R. Haymon, R. Hessler, T. Juteau, M. Kastner, R. Larson, B. Luyendyk, J. D. Macdougall, S. Miller, W. Normark, J. Orcutt,

and C. Rangin, East Pacific Rise: hot springs and geophysical experiments, Science, 207, 1421-1433, 1980.

Wait, J. R., The electromagnetic fields of a horizontal dipole in the presence of a conducting half-space, Can. J. Phys., 39, 1017-1028, 1961.

Young, P. D., The method of Frieman and Kroll for the calculation of electromagnetic fields and its application to data inversion, SIO Reference number 81-15, 1981.

Young, P. D., and C. S. Cox, Electromagnetic active source sounding near the East Pacific Rise, Geophys. Res. Lett., 8, 1043-1046, 1981.

MANDATORY DISTRIBUTION LIST

FOR UNCLASSIFIED TECHNICAL REPORTS, REPRINTS & FINAL REPORTS

PUBLISHED BY OCEANOGRAPHIC CONTRACTORS

OF THE OCEAN SCIENCE AND TECHNOLOGY DIVISION

OF THE OFFICE OF NAVAL RESEARCH

Department of Defense

Office of the Secretary of
  Defense (3)
Assistant Director of Defense
Research & Engineering
Washington, D.C.   20301

Navy

Office of Naval Research (3)
Code 460
Arlington, VA   22217

Office of Naval Research
Code 480
Arlington, VA   22217

Office of Naval Research
Code 102 B
Arlington, VA   22217

Office of Naval Research
Commanding Officer
1030 East Green Street
Pasadena, CA   91101

Naval Ocean Research
& Development Activity
NORDA, Code 300
NSTL Station
Bay St. Louis, MS   39529

Naval Research Laboratory (6)
Library, Code 2620
Washington, D.C.   20375

U.S. Naval Oceanographic Office
Library, Code 8170
NSTL Station
Bay St. Louis, MS   39529

Other Government Agencies

Defense Documentation Center (12)
Cameron Station
Alexandria, VA   22314

National Oceanic & Atmospheric
  Administration
National Oceanographic Data Center
Washington Navy Yard
Rockville, MD   20852